Macromolecular Rheology

Evelyne van Ruymbeke[1] *and Dimitris Vlassopoulos*[2,3]

[1] *Bio and Soft Matter, Institute on Condensed Matter and Nanosciences (IMCN), Université catholique de Louvain (UCL), Louvain-La-Neuve, Belgium*
[2] *Institute of Electronic Structure & Laser, Foundation for Research and Technology Hellas (FORTH), Heraklion, Crete, Greece*
[3] *Department of Materials Science & Technology, University of Crete, Heraklion, Crete, Greece*

1 Introduction

To optimize the processing conditions of polymers it is imperative to have a good understanding of their rheology. Concomitantly, the desired enhanced performance of materials is often associated with their mechanical properties. Let us take a specific example, the sheet blowing process for the production of greenhouse films. The polymer mixture is first extruded through an annular die in order to obtain a macroscopically homogeneous material. At the exit, compressed air is blown, and a tubular film bubble is formed, which is driven into two counterrotating nip rolls with the help of collapsing boards or guide rolls [1, 2]. This process is possible only because of the shear thinning at the extrusion stage to ensure flow of macroscopically homogeneous material and strain hardening at the bubble formation and rolling stages to ensure film stability and uniformity without sagging. Hence, the efficient operation of such a process renders the knowledge of viscoelastic material functions (dynamic moduli, shear viscosity, and normal stresses) necessary. They serve as inputs to constitutive models which are used in the control units in order to adjust the final product based on the specifications. Moreover, they are the key ingredients for designing new materials with optimized flow properties or mechanical strength. Rheology, the science of flow and deformation of matter, is central to tailoring the processing and performance of polymers and composites. The polymers used in applications have typically large molar masses and as a result they form networks which represent topological constraints that severely retard their motion. These constraints are called entanglements and have been quantitatively described by the tube model [3, 4]. Since that development, the field has exploded. Today, molecular constitutive equations are available which link the macroscopic (linear and nonlinear) viscoelastic properties of (linear or branched) polymers to their molecular characteristics. This is exactly the goal of

Macromolecular Engineering: From Precise Synthesis to Macroscopic Materials and Applications, Second Edition. Edited by Krzysztof Matyjaszewski, Yves Gnanou, Nikos Hadjichristidis and Murugappan Muthukumar.

DOI: 10.1002/9783527815562.mme0034

macromolecular rheology, which has a huge impact on both polymer physics and technological applications. The present article provides the main ingredients for understanding the development and use of such models and forms the basis for exploring relaxation mechanisms in polymer-based systems. It starts with the definitions of rheometric material functions and linear viscoelasticity to set the stage for the subsequent discussion. The latter is focused on the dynamics of flexible linear and star polymers, which represent the two pillars for analyzing the viscoelastic response of complex macromolecular architectures. The relaxation mechanisms are explained in detail. Based on this background, a brief discussion of the viscoelastic response of branched polymers follows. The entire presentation is limited to amorphous polymers with particular emphasis on melts. The framework for understanding the nonlinear rheological response (which is directly relevant to processing) is also discussed with emphasis on the state-of-the-art experimental approaches and modeling challenges. Semicrystalline, semiflexible, or rod-like polymers (forming liquid crystalline mesophases) are not discussed, neither are the instabilities (such as wall slip and shear banding) and the fracture mechanisms. Key references concerning these topics are given where appropriate. Finally, some applications of interest to the industrial practice are briefly presented.

2 Basic Elements of Rheological Measurements

The viscoelastic characterization of polymers involves two types of measurements: the linear response where the thermally activated motion of polymers is detected at different length (and respective time) scales, and the nonlinear response where the material functions under the action of external fields that induce conformational changes are probed. Among the different types of imposed deformation, the most popular are shear and uniaxial extension. Note that applications involve complex flows combining shear and extensional deformations. From the continuum hypothesis viewpoint, a specimen is sheared or extended along direction 1 as shown schematically in Figure 1.

Under shear, the different regimes of viscoelastic response can be described schematically in a generic plot of amplitude of deformation γ_0 against normalized rate of deformation. The latter is the frequency ω of oscillatory shear deformation or the rate $\dot{\gamma}$ of steady shear deformation normalized with the relaxation time τ of the viscoelastic material, known as Deborah ($\mathrm{De} = \tau\omega$) or Weissenberg ($\mathrm{Wi} = \tau\dot{\gamma}$) number, respectively. This kind of representation, depicted in Figure 2, is generally known as Pipkin diagram [5]. Note that this representation is very general, and in practice, one should use either De or Wi in the horizontal axis. These two dimensionless numbers are different and typically they are linked by $\mathrm{Wi} = \gamma_0 \mathrm{De}$, where γ_0 is the amplitude of oscillatory deformation. Also, in the vertical axis the amplitude can γ_0 be or γ (say imposed strain or the product $\dot{\gamma}t$, with t being an experimental time). There are different versions of Pipkin diagrams [4, 5], but all attempt at representing the regimes of linear and nonlinear viscoelastic response. For viscoelastic fluids such as polymers, the limit of low rates corresponds to viscous behavior, whereas very high rates correspond

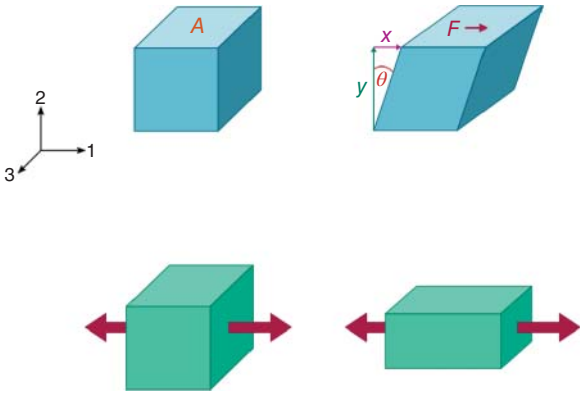

Figure 1 Schematic illustration of shear (top) and extensional (bottom) deformations of a cubic material element along direction 1. In the case of shear, which is imposed by applying a force F on a surface A, the velocity in direction 1 varies along the gradient direction 2, whereas 3 is the neutral direction; the strain is given by $\gamma = \tan\theta = x/y$, and its rate is the shear rate, given by the velocity gradient. In the case of uniaxial extension, the material extends along direction 1 and shrinks (equally) in directions 2 and 3, preserving its overall volume.

Figure 2 Pipkin schematic diagram indicating the different regimes of viscoelastic response (see text for explanations about the axes).

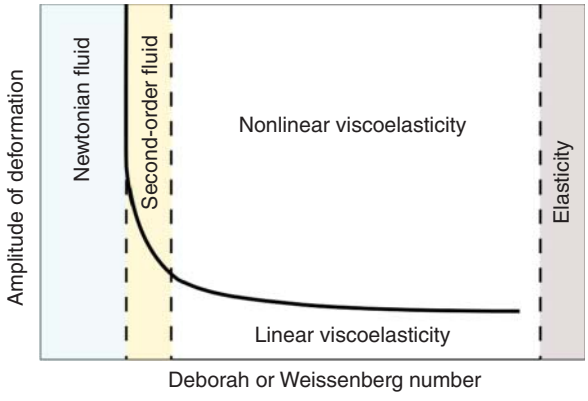

to elastic behavior. Note again that there is a distinction between oscillatory frequency (in a dynamic test) and rate (for example, in an imposed shear-rate test). This will be further discussed below in the context of the Cox–Merz rule [4]. In the lowest rates, Newtonian response is attained [4–6], and the transition to nonlinearity is marked by the weakest nonlinear fluid model, the second-order fluid. Linear viscoelastic responses are also associated with small values of strain deformation. The linear regime serves for characterizing the material in terms of equilibrium properties, whereas the regime of interest in terms of processing is that of intermediate rates and large deformations. The so-called viscometric flows (typically materialized in a rheometer) cover the linear and part of the nonlinear (but not in its entirety) regimes.

A concise summary of typical rheometric measurements and their interrelation is illustrated in Figure 3: Panel (a) represents the time-dependent stress relaxation modulus $G(t)$ at different strains which increase in the direction of the arrow.

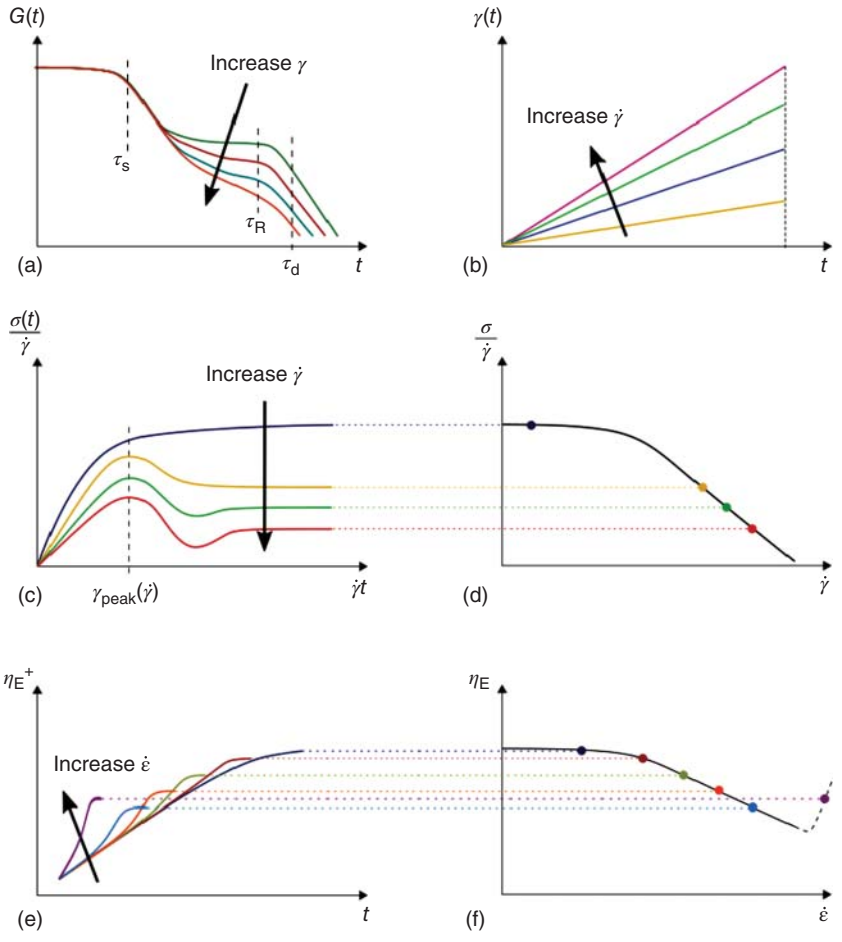

Figure 3 Schematic illustrations of shear and extensional tests. (a) Time-dependent stress relaxation modulus $G(t)$. (b) Time-dependent strain at different imposed shear rates during a constant shear-rate experiment. (c) Transient viscosity ($\sigma/\dot{\gamma}$), known as shear stress growth coefficient, as function of the strain ($\dot{\gamma}$t) for different applied shear rates $\dot{\gamma}$. (d) The values of the steady-state viscosity from the transient experiments of (c) are plotted against shear rate. (e) Extensional stress growth coefficient as a function of time in uniaxial extension for different extensional rates $\dot{\varepsilon}$. (f) The obtained steady-state uniaxial extensional viscosities from (e) are plotted against extensional rate. Details are discussed in the text.

At the lowest strain, the response is linear (i.e. it is the Fourier transformation of the dynamic oscillatory tests at small strain amplitudes), and the plateau modulus typically corresponds to the entanglement regime [6, 7]. The dashed lines represent the characteristic relaxation time: segmental (τ_s), Rouse (τ_R), and terminal (τ_d). The short-time slope (above τ_s) is −0.5, and the long-time slope (in linear regime beyond τ_d) is −1. As the strain γ increases, the modulus becomes dependent on both time and strain, $G(t, \gamma)$. Note that here we focus on the postglass regime only, i.e. plateau and terminal flow. Panel (b) shows the time-dependent strain at different imposed shear rates (increasing in the direction of the arrow)

during a constant shear-rate experiment. In panel (c), the shear stress growth coefficient ($\sigma/\dot{\gamma}$) is plotted against the strain ($\dot{\gamma}t$) for different applied shear rates (increasing in the direction of the arrow). The peak strain is indicated by the dashed line. Then, in panel (d), the values of the steady-state viscosity from the transient experiments of panel (c) are plotted against shear rate. A transition from low-rate Newtonian plateau (zero-shear viscosity) to higher rate shear thinning is observed. Panel (e) shows the uniaxial stress growth coefficient, $\eta_E^+(t)$, as a function of time in uniaxial extension (also called transient elongational viscosity) at different uniaxial extensional (or stretch) rates $\dot{\epsilon}$ (increasing from right to the left). The linear response is characterized by a smooth evolution toward a plateau value (zero-rate viscosity), whereas the nonlinear response is characterized by the so-called transient strain (or extension) hardening. Finally, in panel (f), the obtained steady-state elongational viscosities from panel (e), for linear polymers, are plotted against extensional rate, showing a constant zero-rate regime, followed by extensional thinning, which is typically weaker than the shear thinning of panel (d). Note that while the majority of published works indeed show thinning, there are some exceptions showing thickening as will be discussed below (Figure 3e and f). In the case of branched architectures, extensional thickening can also be observed before the thinning regime [4, 8]. The zero-rate viscosity in uniaxial extension is three times larger than in shear. This was demonstrated by Trouton for Newtonian liquids and has been validated for viscoelastic liquids as well [3, 9]. In fact, the ratio of zero-rate extensional to shear viscosities is known as the Trouton ratio. Note that the trends shown are typical, but not all polymers exhibit the same qualitative behavior. Nevertheless, this is a good starting point for appreciating the different types of material interrogation in mechanical tests.

The measurement of rheological properties of polymeric systems poses several challenges. Concerning linear response, the method of choice is small amplitude oscillatory shear, which provides the storage and loss moduli, G' and G'', respectively [6, 7, 9]. Appropriate annealing to the sample and account of various technical issues (such as thermal expansion of tools, transducer compliance, and phase-angle resolution) ensure accurate and reliable measurements. The nonlinear measurements are more complicated and still represent a subject of scientific debates. For simplicity, the description of shear measurements will be limited to (most frequently used) rotational rheometry. Other types of measurements (e.g. capillary rheometry) are extensively discussed in the literature (see, for example Refs. [1] and [10]). A central issue associated with nonlinear shear response is the appearance of artifacts not due to material failure (say degradation) but due to instabilities linked to material-measurement fixture interaction (e.g. wall slip) or flow (e.g. shear banding) or material-flow-environment effects (e.g. edge fracture). This has been reviewed by several authors [3, 4, 8, 9], and while there is no straightforward answer to the question of what is the best way to perform reliable nonlinear measurements for polymer melts (of interest here), a roadmap has emerged. For shear measurements, the cone-partitioned plate (CPP) geometry is an optimum solution for reducing problems associated with edge-fracture and wall slip [10–13]. The former is usually encountered in elastic systems with non-negligible second normal stress, and the latter in such systems with high plateau modulus (typically above 10^5 Pa). The CPP geometry ensures uniform flow with

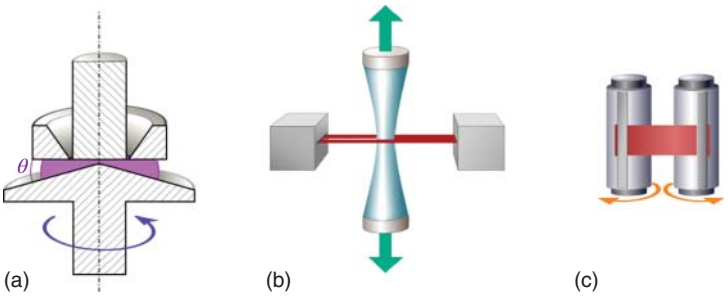

Figure 4 Sketches of experimental devices for measuring nonlinear shear using CPP fixture (a) and uniaxial extension using the FSR instrument (b) or the SER fixture (c). Details are discussed in the text.

constant shear rate by means of the cone, with the sample being overfilled by means of a partition. When the outer edge is distorted (fractures), the transducer connected to the inner top plate (Figure 4) records the torque properly, and this is done so until the fracture propagates inward and reaches the gap separating the inner plate from the partition. Therefore, the fracture is not eliminated, but its influence on the measurement is postponed instead, giving the possibility to obtain reliable data over a range of shear rates until eventually the measurement is ruined by the propagating edge distortion. In fact, reliable data are obtained from transient measurements, which allow obtaining steady-state values of stress or viscosity unambiguously [11, 12, 14–16]. At the same time, the presence of the partition (and the associated normal force) acts against wall slip. Further details concerning the measurements of shear and both normal stresses can be found in Refs. [11, 12, 15, 16].

Concerning extensional rheology, we address here only uniaxial extension, also referred to as elongation. The main challenges faced in these measurements are ensuring true uniaxial conditions and reaching high strains. The state of the art is the so-called filament stretching rheometer (FSR) where a properly treated specimen (annealed and prestretched) is deformed at a certain rate, and the mid-diameter is monitored by means of a laser and a feedback control loop, which ensures that its reduction over time is the expected one for uniaxial deformation [17]. On the other hand, the Sentmanat extensional rheometer (SER) is a fixture mounted on a rheometer, consisting of two counterrotating drums that can stretch films easily but without an accurate control of uniaxial conditions and without reaching as high Hencky strains as the FSR [18]. Further details about the extensional experiments can be found in Refs. [17–19].

3 Linear Viscoelastic Measurements

The linear response of a polymer after a small step strain is typically described by the relaxation modulus $G(t)$, the strain-independent ratio of the stress to the step-strain amplitude (Figure 3a). Alternatively, it is very convenient and useful to apply a small amplitude oscillatory interrogation in the material and follow

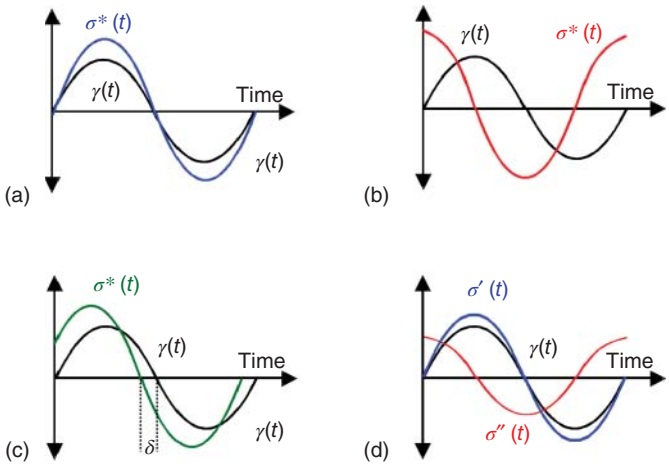

Figure 5 Schematic representations of the oscillatory deformations: applied strain $\gamma(t)$ and responding complex stress $\sigma^*(t)$. (a) Elastic solid with in-phase response. (b) Viscous liquid with a (90°) out-of-phase response. (c) Viscoelastic fluid with a response characterized by a phase angle δ. (d) Decomposition of the viscoelastic stress response (c) into in-phase (σ') and out-of-phase (σ'') components.

its response [6]. A sinusoidally varying strain is routinely applied, with a small amplitude γ_0 in the linear viscoelastic regime and a frequency ω, which represents the inverse time of experimental observation (Figure 5). Depending on the value of ω with respect to the characteristic inherent time of the material (Deborah number), such an experiment probes material response at different times, hence length scales. Therefore, an oscillatory test provides the relaxation spectrum of the material and is often called mechanical spectroscopy. In the linear regime, the stress (needed to ensure a sinusoidal deformation) is also sinusoidal but is shifted by a phase angle δ, whose value ranges between 0° in the case of a purely elastic response and 90° in the case of a purely viscous response. Consequently, as illustrated in Figure 5d, this stress function can be decoupled into two sinusoidal curves, one being in phase with the deformation and the other being in phase with the rate of deformation. These two contributions represent the storage and loss moduli, respectively. The strain, stress, and phase angle can be written as [6]

$$\gamma(t) = \gamma_0 \sin(\omega t) \tag{1}$$

$$\sigma(t) = \sigma_0 \sin(\omega t + \delta) = \sigma_0 \cos(\delta)\sin(\omega t) + \sigma_0 \sin(\delta)\cos(\omega t) \tag{2}$$

$$\begin{aligned}\sigma(t) &= \gamma_0[G'(\omega)\sin(\omega t) + G''(\omega)\cos(\omega t)] \\ &= \gamma_0 G^*(\omega)\,[\cos(\delta)\sin(\omega t) + \sin(\delta)\cos(\omega t)]\end{aligned} \tag{3}$$

$$\tan\delta = \frac{G''}{G'} \tag{4}$$

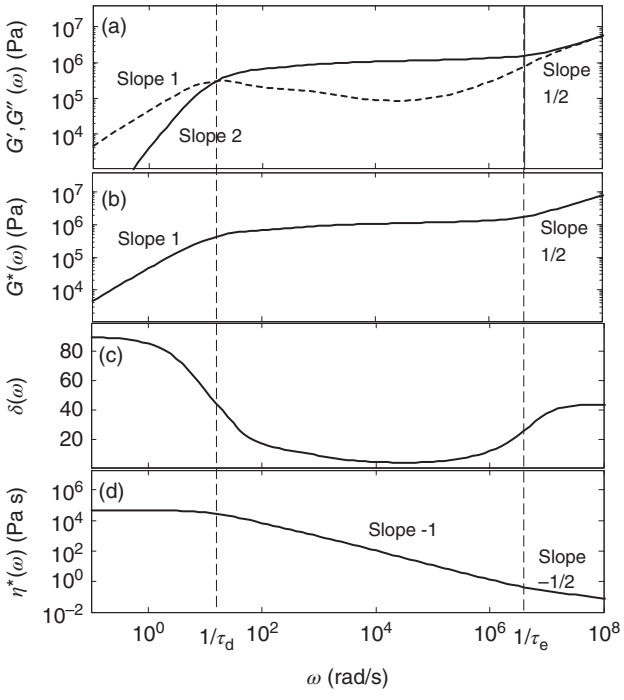

Figure 6 Linear viscoelastic spectra of an entangled polymer (see text for details). Viscoelastic material functions are plotted against frequency: (a) Storage and loss moduli. (b) Complex modulus. (c) Phase angle. (d) Complex viscosity.

The modulus can also be defined based on the complex viscosity, $\eta^*(\omega)$:

$$\eta^*(\omega) = \frac{G^*}{\omega} \tag{5}$$

$$G'(\omega) = \eta''(\omega)\omega \tag{6}$$

$$G''(\omega) = \eta'(\omega)\omega \tag{7}$$

The zero-shear viscosity, η_0, can then be defined as the complex viscosity determined at a frequency low enough to ensure that the response of the sample is purely viscous ($\eta^* = \eta'$, $\eta'' = 0$):

$$\eta_0 = \lim_{\omega \to 0} \frac{G''(\omega)}{\omega} = \int_0^\infty G(t)\mathrm{d}t \tag{8}$$

It is instructive to have a closer look at the dynamic oscillatory response of a simple linear flexible polymer of large molar mass in the entanglement regime. Figure 6 depicts the predicted moduli, phase angle, and complex viscosity for a polybutadiene (1,4-addition) with 100 kg mol^{-1} or $Z \approx 55$ entanglements. The predictions are based on tube modeling (discussed below) and are entirely consistent with experimental measurements [20, 21]. Here, we outline the basic

features of the mechanical spectra. The entanglement regime is characterized by the entanglement (or rubbery) plateau $G' \sim \omega^0 > G''$, between frequencies $\omega_e = 1/\tau_e$ and $\omega_d = 1/\tau_d$, marking the onset and the end (onset of terminal relaxation or flow) of the entanglement network, respectively (Figure 6). At times shorter than the entanglement regime, $t < \tau_e$, the local polymeric response does not "feel" the presence of the physical network since the associated length scale is shorter than an entanglement segment: this is the high-frequency Rouse regime where ideally both moduli collapse and exhibit a power-law dependence on frequency with an exponent of ½. We mention "ideally" because in reality this regime overlaps with, and is often influenced by, the faster segmental relaxation (not shown in Figure 6 since it is not part of the tube and Rouse models), and as a result, the values and frequency dependence of the moduli can be slightly affected [22]. Finally, at times beyond the terminal crossover of moduli, the polymer is completely relaxed, and the classic Maxwell scaling applies $G'' \sim \omega > G' \sim \omega^2$ [6, 7]. The complex modulus G^* reflects the predominance of (elastic or viscous) response in the different regimes, and its frequency dependence is characterized by the power-law exponents of ½, 0, and 1 in the Rouse regime, the entanglement network, and the terminal regime, respectively. The frequency-dependent phase angle follows a similar trend, being very low in the elastic-dominated regime and approaching 90° in the viscous-dominated regime. Finally, the complex viscosity exhibits a Newtonian plateau in the terminal regime and thins in the entanglement regime with a slope of −1, reflecting the entanglement plateau. Then, a weaker thinning with slope of −1/2 is reached, which characterizes the high-frequency regime. The viscosity thinning is directly associated with the spectroscopic nature of this representation, i.e. the fact that different length scales are responsible for the viscoelastic response at different frequencies.

The linear viscoelastic spectrum of a polymer such as that of Figure 6 extends over a huge range of frequencies and moduli, beyond the instrumental capabilities. There exist different possibilities to obtain the experimental spectrum, the most popular being the empirical time–temperature superposition, TTS [6]. Given the experimental frequency window in a typical rheometric study (usually from 100 to 0.01 rad s^{-1}), faster or slower parts of the relaxation spectrum can be brought into the window by heating or cooling the sample, respectively. The obtained linear viscoelastic responses at different temperatures are then shifted with respect to a selected reference temperature onto a master curve. This established procedure usually works (and is expected to work) for amorphous homopolymers and is also used in the inverse sense as a way to test the quality of the experimental data. For copolymers, polymer blends, semicrystalline polymers, and in the glass transition region, deviations occur and have been used as means to determine transitions. This is not further elaborated here, and the interested reader is referred to Refs. [23–27].

Figure 7a depicts a typical example of an experimental master curve for an entangled linear comb polybutadiene (1,4 addition), which consists of a linear backbone with $Z \approx 28$ entanglements and 17 branches, each with $Z \approx 4$ entanglements [28]. For clarity and to relate with the discussion above in the context of Figure 6, both moduli (G' and G'') and the phase angle are shown. One can clearly observe the entanglement plateau (which has the expected value of about

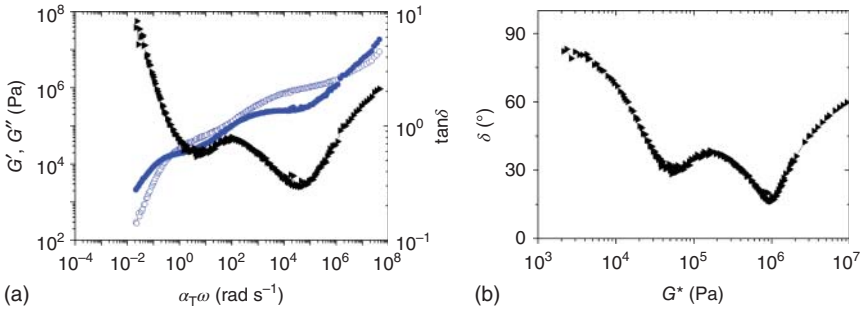

Figure 7 (a) Linear viscoelastic master curve of an entangled linear comb polybutadiene (1,4 addition) from Ref. [28], at a reference temperature of 0 °C. Both frequency-dependent moduli (open symbols for G′) and loss angle (triangles) are shown. Further details are presented in the text and in the reference. Source: Modified from M. Kapnistos, D. Vlassopoulos, J. Roovers and L. G. Leal, Linear Rheology of Architecturally Complex Macromolecules: Comb Polymers with Linear Backbones, Macromolecules, 38, 7852–7862 (2005). (b) Respective representation of the same data in the form of a van Gurp–Palmen plot.

1 MPa [7]). The rubbery plateau region is more complicated than discussed above, characterized by two distinct plateau values. The reason is the particular relaxation of branched polymers, which is hierarchical: for the combs here, the arms with dangling ends relax first, while the backbones remain practically immobile and relax their stress only after the branches have relaxed and effectively diluted the environment (of the backbones). This results in a reduced modulus of the yet unrelaxed backbones and a faster arm relaxation at the lowest frequencies due to the dilution [28, 29]. The concepts of hierarchical relaxation and entanglement dilution will be discussed in the following sections.

The good quality of the master curves can be confirmed and assessed by inspection of the more sensitive frequency-dependent tanδ curve (Figure 7a). Even more sensitive is the so-called van Gurp–Palmen plot [30], which represents the phase angle δ as a function of the complex modulus G^* (Figure 7b). Collapse of the data suggests a very good master curve. The horizontal (a_T) and vertical (b_T) shift factors used to obtain the master curves follow well-defined temperature dependencies. The former is described by the so-called Williams–Landel and Ferry (WLF) empirical Eq. (6), and the latter reflects the variation of density with temperature:

$$\log a_T = \frac{-C_1(T - T_{ref})}{C_2 + T - T_{ref}} \tag{9}$$

$$b_T = \frac{\rho_{ref} T_{ref}}{\rho T} \tag{10}$$

As an example, Figure 8 depicts the horizontal and vertical shift factors for different architectures of polybutadienes, including the data of Figure 7. The excellent overlap of the data confirms that these homopolymers have the same shift factors (same C_1 and C_2 coefficients) independently of their architecture. The values of C_1 and C_2 at the glass transition temperature ($T_{ref} = T_g$) are known for a

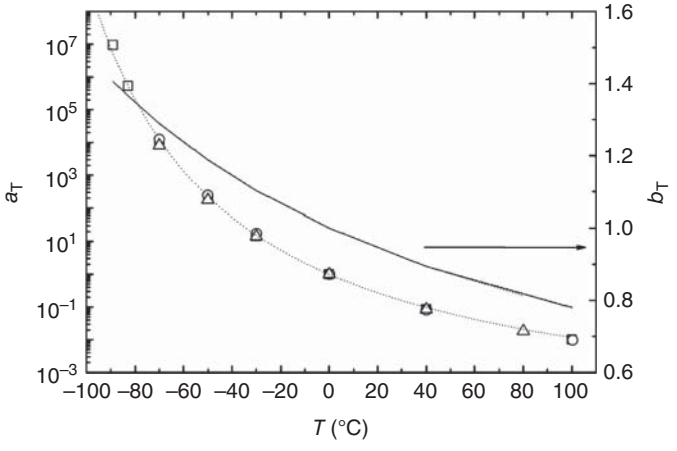

Figure 8 Indicative plot of temperature-dependent shift factors, horizontal (left vertical axis) and vertical (right pointing arrow). Data are shown for different polybutadiene comb polymers, based on Ref. [28] and including the data of Figure 7. Reference temperature is 0 °C. Source: Adapted from M. Kapnistos, D. Vlassopoulos, J. Roovers and L. G. Leal, Linear Rheology of Architecturally Complex Macromolecules: Comb Polymers with Linear Backbones, Macromolecules, 38, 7852–7862 (2005).

huge variety of polymers [6], and in fact, their range is rather limited. This can serve as a way to check the quality of the experimental data.

When the shifted (with respect to T_{ref}) moduli data at different temperatures collapse onto a master curve, the polymer is called thermorheologically simple. The basic reason why the frequency shifting works is that all timescales in the polymer (at different temperatures) are proportional to the segmental time which in turn is proportional to the segmental friction. Hence, the temperature dependence of any time is that of friction. TTS does not work though when there are more than one monomeric friction coefficients with different temperature dependencies and/or other contributions that make the relaxation times more complex and different functions of temperature (for example in the glass regime due to aging or when there is a phase transition) [23–27]. As a consequence of the above, when comparing polymers of the same chemistry but different T_{g} (due to different molar mass of branching structure), the viscoelastic spectra should be compared at isofrictional conditions, i.e. at the same distance $T-T_{\mathrm{g}}$ [31, 32].

The main material parameters can be determined from the experimental moduli and tanδ curves. For example, the minimum of the phase angle in the van Gurp–Palmen plot serves as a sensitive way to determine the plateau modulus. Further methods to extract this important material quantity from experiments are discussed in Ref. [33]. Concerning the determination of relaxation times, often a moduli crossover and the associated peak in tanδ are used. For the terminal time τ_{d}, by extrapolating the G' and G'' data (with slopes 2 and 1, respectively) from low to high frequencies, the inverse of their crossover frequency is a reliable measure. Likewise, for the Rouse time of an entanglement segment τ_{e}, the crossover of the line through the plateau G' and the line through the high-frequency data with a slope of ½ can be used [28].

This, however, is a delicate issue as the high-frequency data may be affected by the segmental relaxation [34]. On the other hand, this time is proportional to the segmental time, hence one could determine it experimentally and backcalculate the monomeric friction which should compare well with the literature value. When the high-frequency regime cannot be determined (for example, in the case of semicrystalline polymers), the τ_e can be calculated from knowledge of the segmental time and monomeric friction [35]. A compilation of data in that regime was recently presented in the literature [22].

4 Linear Viscoelasticity and Influence of Molecular Architecture

These past years, many experimental studies have shown that the viscoelastic response of a polymer melt strongly depends on its molecular structure, which includes both dispersity in molecular weight and dispersity in architecture. Therefore, understanding the relationship between structure and dynamics is of crucial importance in order to determine the role played by specific macromolecular architectures and to design new polymeric systems with desired properties. Furthermore, it allows using rheology as a characterization tool, i.e. determine the molecular structure of a polymer from its viscoelastic properties. In this direction, several coarse-grained models have been developed, which describe the relaxation of macromolecules at a mesoscopic scale. Most are based on the tube-model theory [3]. The main idea behind this mean-field model is to reduce the complex dynamics of interchain topological interactions to a single-body process, where the molecular environment of an observed chain (usually called the "test" chain) is represented by an effective tube which confines the chain. The fact that in such a situation a test chain is surrounded by a very large number of other chains (topological constraints) justifies the mean-field approach.

In this section, the main viscoelastic properties of linear chains, star polymers, and more complex architectures are discussed and rationalized, based on the tube picture [3, 4, 7, 9]. The different relaxation processes of unentangled and entangled polymers subjected to a linear deformation, namely, Rouse relaxation, reptation, contour length fluctuations (CLF), arm retraction, and constraint release (CR) mechanisms, are described, along with the way they depend on the molecular characteristics such as the detailed structure of the macromolecules, their molar mass, their polydispersity (PD), and their concentration. In order to understand the relaxation dynamics of entangled polymers, it is convenient, first, to discuss the viscoelastic properties of model polymers such as nearly monodisperse samples in the melt state or diluted in oligomers. Examples of such polymers, which have been studied during these past two decades, are presented in Figure 9. These macromolecular architectures, which have been obtained via anionic polymerization, are linear chains, star, H, pom-pom, comb, Cayley-tree, ring, and star-comb molecules [4, 7, 9, 36]. The results can then be extended to the characterization of polydisperse and not well-defined systems, as often obtained with industrial processes.

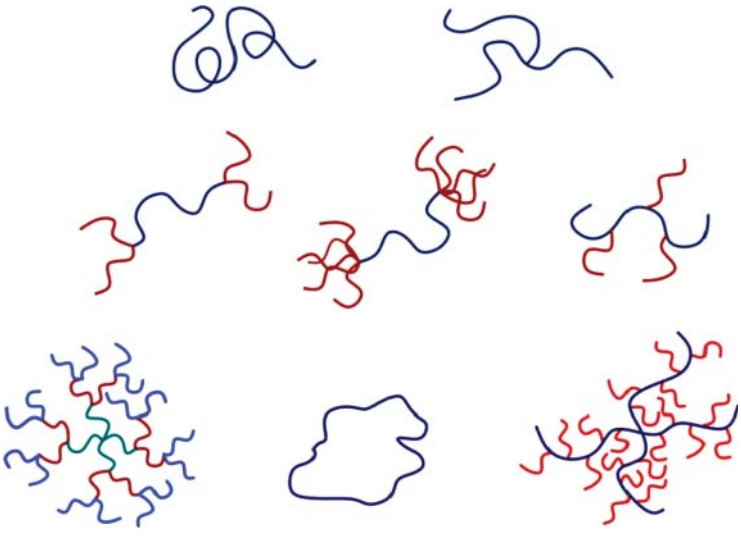

Figure 9 Representation of well-defined macromolecular architectures. From top left: linear, star, H, pom-pom, (linear) comb, Cayley tree, ring, and star comb. Different colors indicate distinct branches or generations.

4.1 Linear Viscoelastic Properties of Linear Polymers

4.1.1 Unentangled Linear Polymers

Here, a polymer melt (or solution) consists of independent, noninteracting chains. The relaxation of such unentangled chains is well described by the Rouse model [7], which considers an independent chain as a sequence of dumbbells made of beads connected with springs (Figure 10). Usually, each of these dumbbells represents a Kuhn segment [7]. In order to describe the stress relaxation of the chain, the length scale at which the chain configuration has been renewed in comparison to the initial configuration must be determined at each time step. Since at very short time ($t \approx 0$) the chain configuration is nearly identical to its initial configuration, each Kuhn segment contributes an amount of energy kT to the stress needed to keep the chain deformed, with k being the Boltzmann constant. Therefore, at this time, the corresponding modulus $G(t \approx 0) = \nu kT\ n$, with ν being the number density of chains, and n the total number of Kuhn segments per chain. When time is getting longer, as illustrated in Figure 10, the orientation of the chain segments slowly loses its correlation with the initial orientation, first at a very local length scale and later at a larger length scale. These different length scales define the different modes of the Rouse relaxation: for a chain of molar mass M, the mode "p" corresponds to the Rouse relaxation of chain segments of molar mass (M/p) and is therefore associated to a relaxation modulus $G(\tau_p) \approx \nu kT\ p$.

The necessary time for such segments to renew their configuration (i.e. relax), τ_p, is proportional to the relaxation time of a Kuhn segment, τ_0, and scales with the square of the number of Kuhn segments they contain:

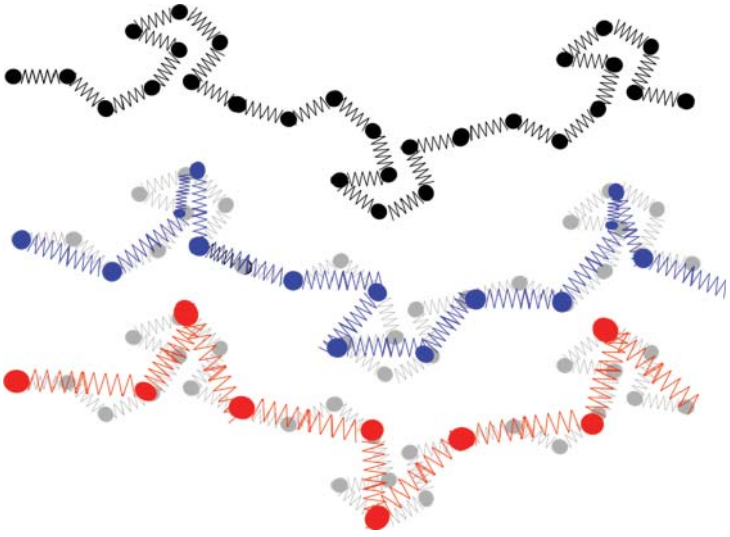

Figure 10 Schematic illustration of the Rouse modes, at the level of each Kuhn segment (represented by the dumbbells in black on top and gray subsequently), two Kuhn segments (blue), and three Kuhn segments (red). With time, the length of the molecular segments that have renewed their configuration is increasing, until the whole chain is fully relaxed (not shown).

$$\tau_p = \frac{\zeta_0 b^2 n^2}{3\pi^2 kTp^2} \approx \tau_0 \left(\frac{n}{p}\right)^2 = \frac{\tau_R}{p^2}, \quad \text{for } p = 1, 2, \ldots, n. \tag{11}$$

where ζ_0 is the friction coefficient of one Kuhn segment.

The longest mode, $\tau_R \approx \tau_0 n^2$, which corresponds to the relaxation of the entire chain, is called the Rouse time of the chain (i.e. its longest relaxation time). At time longer than τ_R, the chains are fully relaxed and can diffuse within the sample, while at shorter time t, only the viscoelastic modes faster than the mode $p \approx \left(\frac{t}{\tau_0}\right)^{-\frac{1}{2}} n$ relax, which leads to a relaxation modulus that scales with $t^{-1/2}$. The Rouse relaxation of unentangled polymers is illustrated in Figure 11 for linear chains of same nature (chemistry) but with different molar masses. As long as the chains are relaxing locally ($t < \tau_R$), the stress level is independent of the molar mass of the entire chains. However, the end of this regime, i.e. the terminal relaxation time of these unentangled chains, is determined by their Rouse time, τ_R, which depends on M in a quadratic way.

Similarly, the relaxation modulus of an unentangled chain can be determined by considering that each unrelaxed Rouse mode contributes energy kT (per chain) to the stress (i.e. at time τ_p, the chain contains p unrelaxed segments of mass M/p, which corresponds to p unrelaxed modes (1, 2, …, p)). In such a case, the relaxation modulus can be approximated as

$$G(t) = kT\,\nu \sum_{p=1}^{n} \exp\left(\frac{-2t}{\tau_p}\right) = \frac{\rho RT}{M} \sum_{p=1}^{n} \exp\left(\frac{-2t}{\tau_p}\right) \tag{12}$$

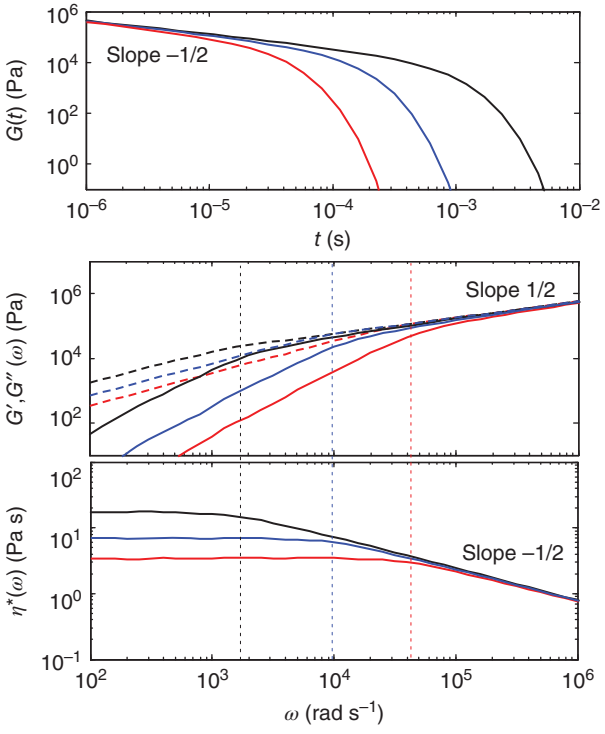

Figure 11 Representative linear viscoelastic spectrum predicted by the Rouse model for unentangled linear chains of the same nature but with different molar mass: weight-average molar mass $M_w = 20$ kg mol^{-1} (red), 40 kg mol^{-1} (blue), or 100 kg mol^{-1} (black). The dashed lines correspond to the characteristic terminal frequency ($\omega = 1/\tau_R$).

4.1.2 Entangled Linear Polymers

Several relaxation mechanisms are needed in order to fully describe the relaxation of an entangled polymer. We describe here the relaxation processes observed with linear entangled chains.

4.1.2.1 Rouse Relaxation and Equilibrium State

Entangled chains cannot move freely in all directions due to their interactions with other chains, which they cannot cross and with which they create entanglements [3, 7]. The space they can explore by thermal motions is therefore restricted. Consequently, within these constraints only the fast Rouse relaxation modes can take place since they involve local motions of chain segments (Figures 10 and 12). At this short time (or length) scale, the mutual influence between the molecules can be ignored, and entangled polymers relax similarly to unentangled chains, i.e. according to the Rouse model. However, at longer times, the chains feel the topological interactions. Their entanglements act as temporary physical cross-links, which prevent the longest Rouse modes to fully relax. As illustrated in Figure 12, the longest subchains that can relax by Rouse motion are called the entanglement segments. They have a molar mass

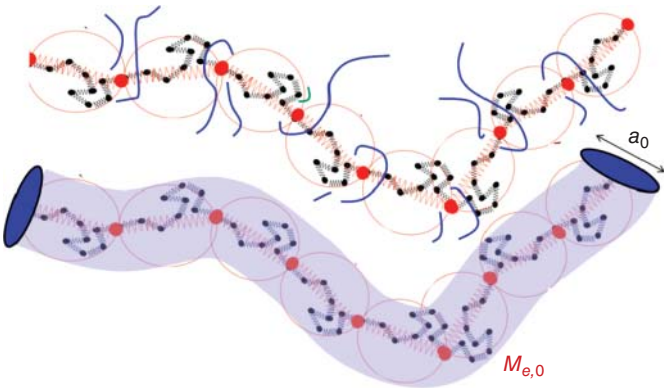

Figure 12 Definition of the entanglement segments. They are the longest subchains that can relax by Rouse process and are represented by the red circles (blobs). Their molar mass is M_e, while their corresponding (Rouse) relaxation time, τ_e, is equal to $\tau_0 (M_e/m_0)^2 = \tau_0 n_e^2$. The restricted space around a chain is represented by a tube diameter a_0.

equal to M_e and contain n_e Kuhn segments, while the chain contains $Z = M/M_e$ entanglement segments.

At time τ_e, when the entanglement segments relax by Rouse process, the relaxation modulus is equal to $G_e = G(\tau_e) = \nu kTZ = \frac{\rho RT}{M} Z = \frac{\rho RT}{M_e}$ and cannot decrease further by full Rouse relaxation (FR). However, around one-fifth of this modulus is lost due to the partial Rouse relaxation of the longest Rouse modes, along their backbone, i.e. in one direction [4, 7, 37]. These partial Rouse relaxation modes are called the longitudinal Rouse modes (LR). After both Rouse and LR relaxation, the chains reach another state, where they cannot relax further temporarily. The corresponding modulus is called the plateau modulus, G_N^0, and is inversely proportional to the average molar mass between two entanglements, M_e [3, 7]:

$$G_N^0 = \frac{4}{5} \frac{\rho RT}{M} Z = \frac{4}{5} \frac{\rho RT}{M_e} \tag{13}$$

Note that while this definition of plateau modulus is typically used in the models, the experimental equilibrium plateau modulus is often considered as that before the LR relaxation, i.e. at the onset of the plateau (after) and $G_e = \frac{\rho RT}{M_e} = \frac{b^3}{\nu_0} \frac{kT}{a_0^2 b}$, where ν_0 is the volume of a lattice site occupied by a monomer, b the monomer, and a the tube diameter [7, 38].

Figure 13 depicts the time-dependent relaxation modulus and the respective frequency-dependent storage modulus of an entangled linear polymer relaxing only by Rouse and LR processes. The polymer is monodisperse polybutadiene 1,4-addition with molar mass 100 kg mol^{-1}, PBD100k. In such a case, $G(t)$ is well described as

$$G(t) = G_{FR}(t) + G_{LR}(t) + G_N^0$$

$$G_{FR}(t) = \frac{\rho RT}{M} \sum_{p=Z+1}^{n} \exp\left(\frac{-2t}{\tau_p}\right)$$

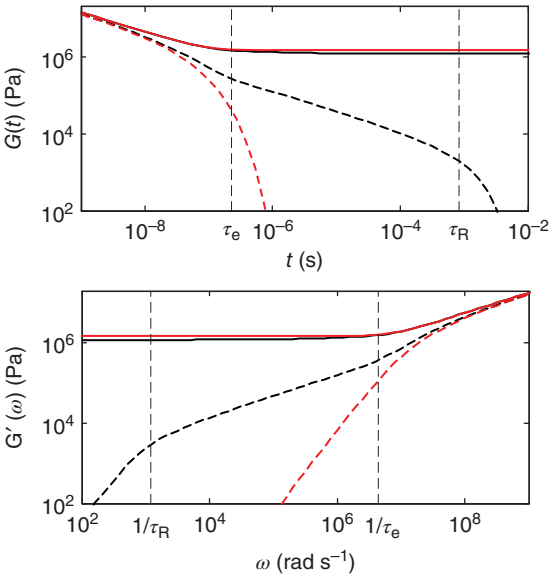

Figure 13 Relaxation modulus (top) and storage modulus of 1,4 PBD100k, taking into account the FR of the entanglement segments with (black curves) or without (red curves) considering the influence of the longitudinal modes. The black and red dashed curves show the contribution of both the FR and LR modes or of the FR modes only, respectively. At long times (low frequencies), the modulus reaches its plateau value G_N^0.

$$G_{LR}(t) = \frac{1}{5}\frac{\rho RT}{M}\sum_{p=1}^{Z-1}\exp\left(\frac{-t}{\tau_p}\right) \tag{14}$$

In the rubbery plateau regime where entangled chains cannot further relax by Rouse process, rather they attain an equilibrium state where the three main material parameters of the tube-model theory are defined: (i) the plateau modulus, G_N^0, (ii) the molecular weight between entanglements, M_e, and (iii) the Rouse time of an entanglement segment (between two constraints) τ_e. The material parameters G_N^0 (or equivalently G_e) and M_e are linked through the rubber elasticity relationship given in Eq. (13). These parameters do not depend on the architecture nor on the molar mass of the polymer. Typical values of G_e and M_e are given in Table 1 for some frequently studied polymer melts. Some differences between reported data are noted. Hence, it is important to use one value consistently and characterize the measured sample well. Note that Eq. (13) suggests a weak temperature dependence, so the values are reported at specific temperatures [7].

At this stage of the relaxation process, the chain representation can be even more coarse-grained, considering the entanglement segments as the smaller units (represented by the red dumbbells in Figure 12). The most probable curvilinear path length of the chain at this equilibrium state, L_{eq}, is thus equal to Zl, with l being the length of an entanglement segment. The average diameter of the tube confining the chain (see Figure 12), a_0, can also be determined. Since the tube is an average object that represents the constraining effects of the surrounding macromolecules, its diameter is considered constant along the chain and for all the chains present in the sample. Assuming Gaussian chains moving in a tube of diameter a_0, L_{eq} and a_0 are related through the relation:

$$R^2 \approx L_{eq}a_0 = Z\,l\,a_0, \tag{15}$$

Table 1 Values of the equilibrium plateau modulus and the entanglement molar mass for some polymer melts.

	G_N^0 (Pa)	M_e (kg mol^{-1})
Polystyrene (140 °C)	2×10^5	17
(210 °C)	*1.95×10^5*	*18.5*
Polyisoprene 1,4 addition (25 °C)	3.5×10^5	6.4
	3.8×10^5	*5.9*
Polybutadiene 1,4 addition (25 °C)	1.1×10^6	1.9
	1.2×10^6	*1.96*
Polyethylene (140 °C)	2.6×10^6	1
(190 °C)	*1.95×10^6*	*1.5*
Polydimethylsiloxane (25 °C)	2×10^5	12

Data in italics are taken from C. Liu, J. He, E. van Ruymbeke, R. Keunings and C. Bailly, Polymer, 47, 4461–4477 (2006) [33]. Data from M. Rubinstein and R. H. Colby, Polymer physics, Oxford (2003) [7]; L. J. Fetters, D. J. Lohse, and R. H. Colby, Physical Properties of Polymers Handbook, 447–454 (2007) [39].

where R is the quadratic end-to-end distance of the relaxed chain. On the other hand

$$R^2 = nb^2 = Z\, n_e b^2 = Z l^2. \tag{16}$$

Therefore, $a_0 = l$. In order to fully relax, an entangled polymer chain has to escape from the (stressed) entanglement network via tube renewal (diffusion along the tube). This includes different relaxation processes (reptation, CLF, and CR mechanisms) described in detail in the following section. Accounting for this possible relaxation process, the relaxation modulus can be described as

$$G(t) = G_{FR}(t) + G_{LR}(t) + G_d(t) = G_{FR}(t) + G_{LR}(t) + G_N^0\, F(t) \tag{17}$$

where $F(t)$ is a measure of the relaxation state of the entangled chains, ranging from 1 when the chains are still fully confined in their original (stressed) tube to 0 when the chains have completely renewed their configuration.

4.1.2.2 Reptation

The easiest way for a linear chain to escape from its initial tube is through its thermally activated diffusion along the curvilinear axis of the tube, as illustrated in Figure 14. This relaxation process, which is called "reptation," is well described by a one-dimensional diffusion equation, as shown in Ref. [3]. By moving thermally (Brownian) back and forth along the contour of the tube (often called the primitive path), the chain can slowly escape its initial tube, hence progressively lose its correlation with the initial configuration.

The chain diffuses with a curvilinear diffusion coefficient, D_c, which depends on the total drag of all its constituent monomers and is thus inversely proportional to the number of Kuhn segments, n, and the respective monomeric friction

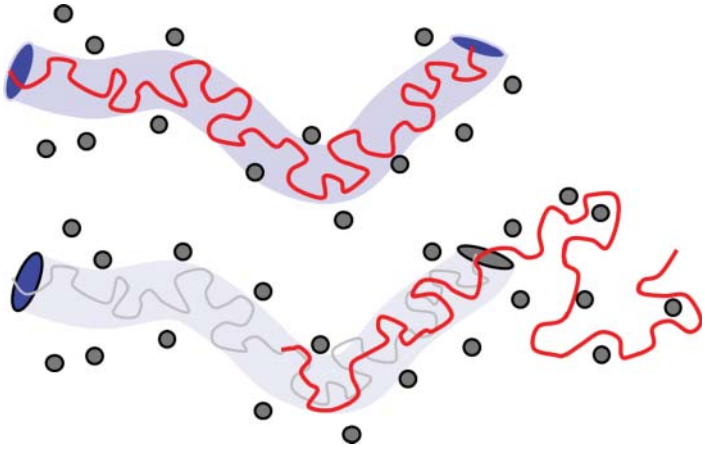

Figure 14 Schematic illustration of the reptation process: the initial tube (top) is being progressively evacuated by the contained red chain that slides curvilinearly back and forth.

coefficient, ζ_0 (through the Einstein law):

$$D_c = \frac{kT}{n\zeta_0} \tag{18}$$

Therefore, the time needed to relax the entire chain by reptation, τ_{rept}, is proportional to the cube of the molecular weight of the test chain:

$$\tau_{rept} = \frac{{L_{eq}}^2}{\pi^2 D_c} = \frac{\zeta_0 {n_e}^2 b^2}{\pi^2 kT}\left(\frac{M}{M_e}\right)^3 = 3\tau_e Z^3 \tag{19}$$

This M^3 dependence of the reptation time must be compared to the M^2 dependence of the Rouse time. The same M^3 scaling is predicted for the zero-shear viscosity of entangled linear polymers, $\eta_0 \approx G_N^0\, \tau_{rept}$. Note that the ratio M/M_e represents the number of entanglement constraints and is usually called "number of entanglements."

The influence of molar mass on the reptation of linear chains is illustrated in Figure 15. If the chains are shorter than a critical molar mass, $M_c \approx 2\, M_e$, they are too short to be entangled and relax fully by a Rouse process.

The probability that a molecular segment has not relaxed by reptation at time t has been determined by Doi and Edwards [3]. The average probability of a chain of mass M to have reptated at time t can be approximated as the time-decreasing exponential function $\exp\left(\frac{-t}{\tau_{rept}(M)}\right)$.

4.1.2.3 Contour Length Fluctuations (CLF)

Initially proposed by Doi, the CLF process is necessary to accurately model the relaxation of linear or branched polymer melts [3, 4, 7]. Occurring at short times compared to τ_{rept}, this process takes into account the fact that the chain extremities have more degrees of freedom compared to inner segments since they are not constrained by the tube (Figure 16). They can easily explore their surrounding and, therefore, relax their orientation at times much shorter than τ_{rept}.

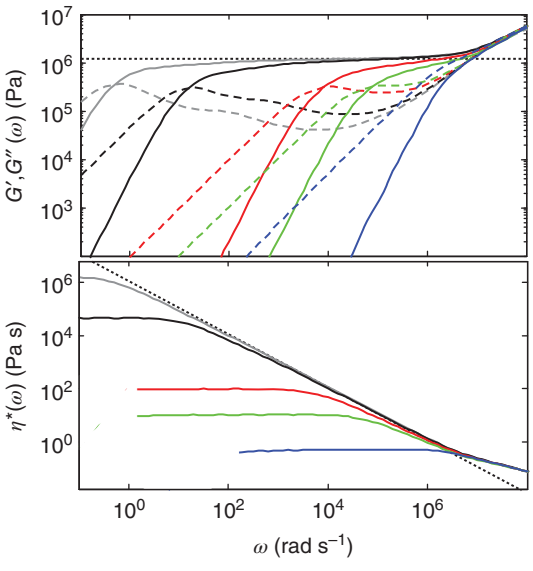

Figure 15 Predicted viscoelastic properties of linear 1,4 PBD chains with $M_w = 3$ kg mol^{-1} (blue), 10 kg mol^{-1} (green), 20 kg mol^{-1} (red), 100 kg mol^{-1} (black), and 300 kg mol^{-1} (gray). The chosen material parameters are $G_N^0 = 1.2$ MPa, $M_e = 1.65$ kg mol^{-1}, and $\tau_e = 2.3 \times 10^{-7}$ s. The shorter polymer is unentangled. The dotted line represents the rubbery plateau [40]. Source: Based on V Shchetnikava, J Slot, E van Ruymbeke, Comparative Analysis of Different Tube Models for Linear Rheology of Monodisperse Linear Entangled Polymers, Polymers 11 (5), 754 (2019).

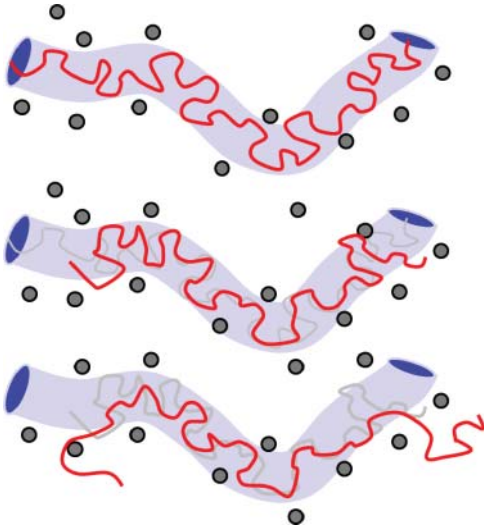

Figure 16 Illustration of the CLF process: the chain ends evacuate fast the outer sections of the tube over time. The time progression of this process is shown from top (initial fully occupied tube to bottom).

This process is a Rouse process, which allows the relaxation of about $\sqrt{Z}$ entanglements at each extremity of the chain [3]. The estimated time to relax a molecular segment localized at a position x along the chain (ranging from 0 at the chain extremity to 1 in the middle of the chain) by CLF is determined as [37]

$$\tau_{\text{early}}(x) = \frac{9\pi^3}{16}\left(\frac{M_a}{M_e}\right)^2 \tau_R\, x^4 \tag{20}$$

Here, the linear chain is treated as a two-arm star polymer with arm molar mass M_a. The CLF speeds up the overall relaxation of the polymer, since the chain fraction relaxed by CLF does not contribute anymore to the length of

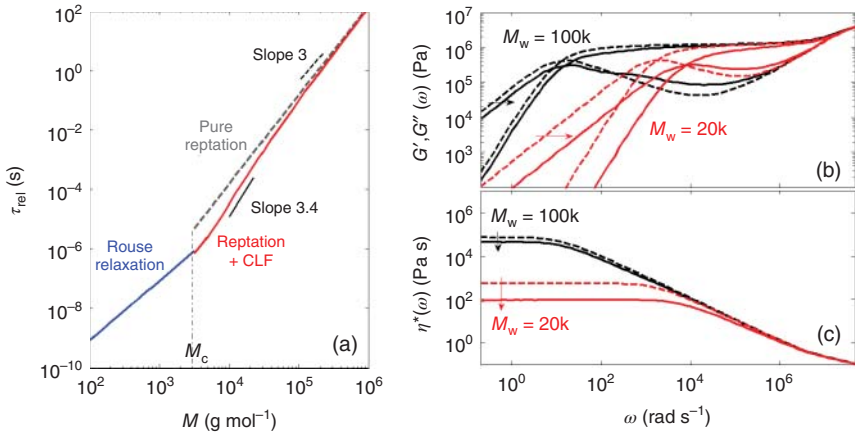

Figure 17 (a) Influence of CLF on the relaxation time of linear 1,4-PBD chains as function of their molar mass. Predicted frequency-dependent viscoelastic moduli (b) and complex viscosity (c) of linear 1,4-PBD chains of $M_w = 20$ kg mol^{-1} (red) and 100 kg mol^{-1} (black) with (continuous curve, Eq. (21)) and without (dashed curve, Eq. (19)) CLF contribution.

the primitive path along which the chains have to reptate in order to relax (see Eq. (19)). According to Doi and Edwards, CLF is at the origin of the $M^{3.2-3.6}$ scaling observed experimentally for viscosity and relaxation time of linear chains as function of their molar mass [4, 7, 9], as illustrated in Figure 17: while the influence of CLF is negligible for very long chains, it strongly reduces the primitive path length and, thus, the relaxation time of a chain containing a moderate number of entanglements. It has been shown in Ref. [37] that the relaxation time of monodisperse linear chains, taking into account both reptation and CLF effects, is well described by

$$\tau_{rel} = \tau_{rept}\left(1 - \frac{3.38}{\sqrt{Z}} + \frac{4.17}{Z} - \frac{1.55}{Z^{3/2}}\right) \tag{21}$$

4.1.2.4 Constraint Release (CR)

In addition to reptation and CLF, a polymer chain can also relax its stress by CR. This process arises from the fact that, unlike the initial consideration of the reptation process in a fixed tube, the molecular environment around a specific chain is also moving and relaxing [41]. Therefore, an entanglement along the tested chain can be lost either if this chain reptates and disentangles, or if another chain involved in the entanglement releases it by diffusion [42]. The CR process will thus speed up polymer relaxation. In the extreme case of long chains diluted in a sea of very short chains, the latter move so fast that they do not constrain the motions of the long chains and can therefore be compared to an oligomeric solvent. It is therefore important to first discuss how an oligomeric solvent is affecting the linear viscoelastic properties of a long linear polymer before discussing the CR process in a polymer melt.

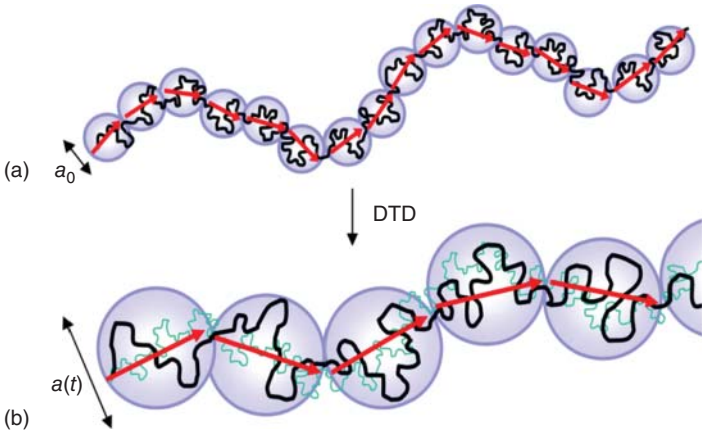

Figure 18 Influence of diluting polymer chains in an oligomeric matrix: (a) melt state and (b) oligomeric solution with polymer concentration *c*. The entanglement segments are represented by the blobs. When diluted, the average number of chain entanglements decreases from Z_{melt} to $Z = Z_{\text{melt}} \cdot c^{\alpha}$. The sequence of red arrows represents the primitive path. Source: van Ruymbeke, E., Masubuchi, Y., & Watanabe, H. (2012). Effective Value of the Dynamic Dilution Exponent in Bidisperse Linear Polymers: From 1 to 4/3. Macromolecules, 45(4), 2085–2098, https://doi.org/10.1021/ma202167q.

4.1.2.4.1 Entangled Polymers Moving in an Oligomeric Matrix Diluting entangled polymers into an oligomeric matrix has a strong effect on their entanglement state: for a polymer concentration, *c*, the average molar mass between two entanglements, M_e, is equal to $\frac{M_{e,melt}}{c^{\alpha}}$, where $M_{e,melt}$ represents the entanglement molar mass in the melt, and α is the dilution exponent [43]. Theoretically, its value should be equal to 1, which is in agreement with many experimental data for polymer melts or solutions in oligomers [9]. However, if the chains are diluted in a real solvent, it has been shown that α can take larger values, up to 4/3 [7, 44]. The influence of diluting a linear polymer into an oligomeric matrix on the number of its entanglements is schematically illustrated in Figure 18. M_e increases with respect to its value in the melt the corresponding Rouse time is $\tau_e = \tau_0 \left(\frac{M}{M_e}\right)^2 = \tau_{e,melt}\, c^{-2\alpha}$.

Furthermore, diluting the polymer also affects its density as $\rho = \rho_{melt}.c$. Considering the effect of dilution on both M_e and ρ, the plateau modulus is found to scale with $c^{1+\alpha}$ [43]:

$$G^0_{N,sol} = \frac{4}{5}\frac{(\rho_{melt}\, c)\, R\, T}{M_e} = G^0_N\, c^{1+\alpha} \tag{22}$$

As illustrated in Figure 18, the length of the primitive path of the chain decreases with decreasing concentration as $L_{eq} = L_{eq,melt}\, c^{\frac{\alpha}{2}}$, while the tube diameter increases as $a_0 = a_{0melt}\, c^{\frac{-\alpha}{2}}$. The consequence of this rescaling is that the reptation and CLF processes speed up. In particular, from Eq. (19), one can conclude that the reptation time scales as [45]

$$\tau_{rept} = \tau_{rept,melt}\, c^{\alpha} \tag{23}$$

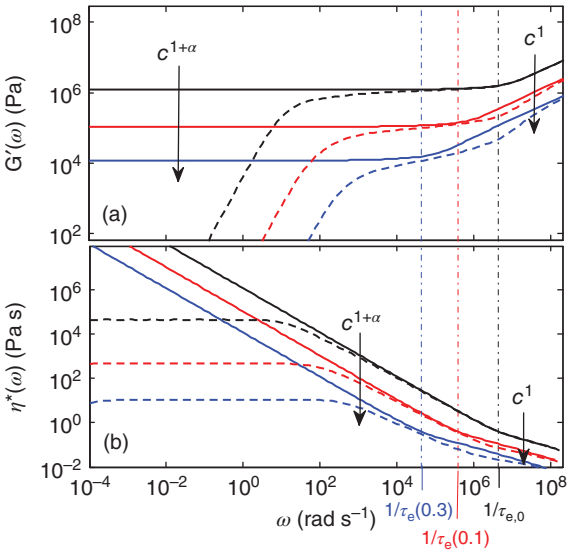

Figure 19 Influence of concentration on the storage modulus (a) and complex viscosity (b) of entangled chains. Model predictions are shown for a linear 1,4-PBD of 100 kg mol^{-1} diluted in oligomers of 4 kg mol^{-1} at $c = 100$ wt% (black), 30 wt% (red), or 10 wt% (blue). The curves have been obtained by accounting (thick dashed curves) or not (continuous curves) for chain relaxation by reptation and CLF.

These important scaling laws are reflected in Figure 19, which depicts the influence of concentration on the high-frequency Rouse regime, the level of the rubbery plateau, and the reptation time. Note that in the Rouse regime, the moduli scale with concentration.

4.1.2.4.2 Entangled Polymers Moving in a Polymer Matrix If part of the molecular environment of a test chain is moving comparatively fast, its constraining effect is reduced, and consequently, the relaxation of the test chain speeds up. While there are several ways to account for this dilution effect within the framework of tube model, the most successful approach is the Dynamic Tube Dilation (DTD) [4, 7, 43]. In the specific case of asymmetric binary blends comprising long and short chains, an additional process, called the Constraint Release Rouse process (CRR), should also be taken into account, in addition to DTD.

The concept of DTD can be explained as follows: At a specific time t, the tube, which represents the topological constraints on a given chain from its molecular environment, should only involve the fraction of chains that are effectively constraining the motion of the test chain at this time, i.e. it should only involve the fraction of chain segments that are not yet relaxed at time t, $\phi(t)$. Thus, the chain segments already relaxed at time t are considered as effective solvent for the chain segments that are not yet relaxed (the respective portion of the tube is not renewed, i.e. it survives). As illustrated in Figure 20a, this leads to an increase in the effective entanglement molar mass, $M_e(t)$, and, consequently, an increase in the effective tube diameter, $a(t)$, with time:

$$M_e(t) = \frac{M_{e,0}}{\Phi_{tube}(t)^{\alpha}} \tag{24}$$

$$a(t) = a_0\, \Phi_{tube}(t)^{\frac{-\alpha}{2}} \tag{25}$$

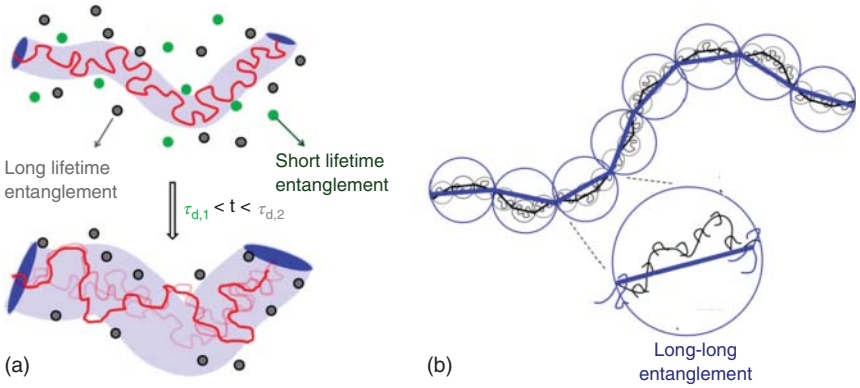

Figure 20 (a) Schematic illustration of the DTD concept. At time *t*, entanglements can be divided into two categories: those that relax before *t* (represented in green) and those with a relaxation time longer than *t* (represented in gray). According to DTD, only the long-lifetime entanglements should be considered as effectively constraining the chain motion. (b) Illustration of the two length scales involved in the description of a long chain in the case of a binary blend of long and short chains [46]. Source: E. van Ruymbeke, V. Shchetnikava, Y. Matsumiya, and H. Watanabe, Dynamic Dilution Effect in Binary Blends of Linear Polymers with Well-Separated Molecular Weights, Macromolecules, 47 (21), 7653–7665, https://doi.org/10.1021/ma501566w.

The reduction in the effective number of entanglements with time also affects the relaxation modulus (after the Rouse relaxation of the entanglement segments):

$$G_{\mathrm{d}}(t) = \frac{4}{5}\frac{(\rho_0\,\phi(t))\,R\,T}{(M_{\mathrm{e}}/\Phi_{\mathrm{tube}}(t)^{\alpha}} = G_N^0\,\phi(t)\Phi_{\mathrm{tube}}(t)^{\alpha} \tag{26}$$

In these equations, the dilation factor $\Phi_{\mathrm{tube}}(t)$ is usually equal to $\phi(t)$, the survival fraction of initial tube at time *t*. However, it can take larger values in specific cases where the tube dilation is slowed down by the so-called CRR [46, 47]. This is typically the case when a large amount of short chains are relaxing in a very short time period, for example with binary blends of long and short chains. In such a case, after the relaxation of the short chains, the long chains cannot occupy their dilated tube instantaneously. The latter becomes effective only after a time $\tau_{\mathrm{e,\,long}}$, which is the necessary time for the segments between two long–long entanglements (i.e. the entanglements involving two long chains, see Figure 20b) to relax by Rouse process, at the rhythm of the disappearance/appearance of the short–long entanglements; thus, $\tau_{\mathrm{e,\,long}} \approx \tau_{\mathrm{short-long}} n_{\mathrm{short-long}}{}^2$.

In addition, the DTD process can also accelerate the reptation and fluctuations mechanisms since the length of the effective primitive path of the tube, $L_{\mathrm{eq}}(t) = L_{\mathrm{eq}}(t=0)\ \{\Phi_{\mathrm{tube}}(t)\}^{\alpha/2}$, is becoming shorter. This is illustrated in Figure 21a, for a set of binary blends composed of long and short chains in different weight fractions, υ_{long} and $\upsilon_{\mathrm{short}}$. It can be observed that the relaxation time of the long component decreases with increasing the fraction of short chains. The low-frequency plateau is also observed to decrease slightly faster than with $\upsilon_{\mathrm{long}}{}^2$, due to the enhanced effect of the CLF in the dilated tube [46].

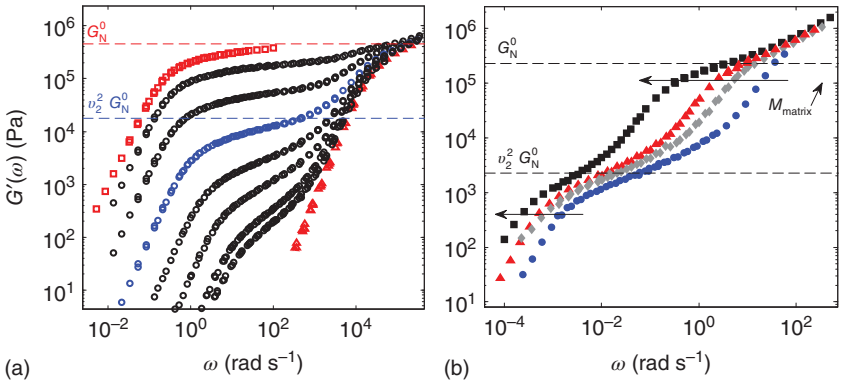

Figure 21 Experimental storage modulus of (a) binary blends composed of long polyisoprene (PI) chains of 329 kg mol^{-1} and short PI chains of 14 kg mol^{-1}, in different fractions ($\upsilon_{long} = 100$ (bulk PI329, □), 70, 40, 20 (blue o), 10, 5, 2, 1, and 0 (bulk PI14, Δ) [46]. Source: van Ruymbeke, E., Shchetnikava, V., Matsumiya, Y., and Watanabe, H. (2014). *Macromolecules* 47 (21): 7653–7665. doi: 10.1021/ma501566w. (b) Binary blends composed of 10 wt% of long PS chains of 820 kg mol^{-1} and 90 wt% of short chains of 8.8 kg mol^{-1} (blue o), 23 kg mol^{-1} (gray ◇), 34 kg mol^{-1} (red Δ), or 73 kg mol^{-1} (black □) [45]. Source: Shahid, T., Huang, Q., Oosterlinck, F. et al. (2017). *Soft Matter* 13 (1): 269. doi: 10.1039/C6SM01083K.

However, it has been shown in the literature that the reptation and CLF of the long chains do not always take place in a dilated tube, as initially proposed in the DTD picture. Indeed, the long chain motion in the dilated tube can occur only at the rhythm of the disappearance/appearance of the short–long entanglements, which can be rather slow if the short chains are not short enough [48, 49]. Therefore, depending on the faster way to relax, the relaxation of the long chains is associated with one of the two length scales illustrated in Figure 20b: either they reptate and fluctuate along the initial primitive path with a characteristic time of an entanglement segment equal to τ_e or they relax along the dilated tube formed by the long–long entanglement segments, but with a characteristic time $\tau_{e,long}$, which depends on the lifetime of the short–long entanglements. Thus, with this dilated tube description, the long chains move along an effectively much shorter backbone, which speeds up their relaxation; however, this is counterbalanced by the relaxation time if a long–long entanglement segment can be much longer than its intrinsic Rouse time. The influence of the short chain relaxation on the relaxation of the long chains is illustrated in Figure 21b: despite the fact that the same long chains are blended in the same proportion in all binary blends, it is observed that their final relaxation time increases with the length of the short chain matrix.

There is a huge body of high-quality experimental data in the literature that illustrate aspects of DTD, typically in long/short polymer mixtures or branched polymers, as will be discussed in the following section. In particular, today, the study of binary blends remains a very active field since it represents a critical test for validating the proposed CR processes. For details, the reader can consult Refs. [9, 29, 41, 43, 49–53].

4.1.2.4.3 Polydisperse Linear Polymers Polydisperse linear polymers also relax by reptation, CLF, and CR processes. However, since the relaxation time of the

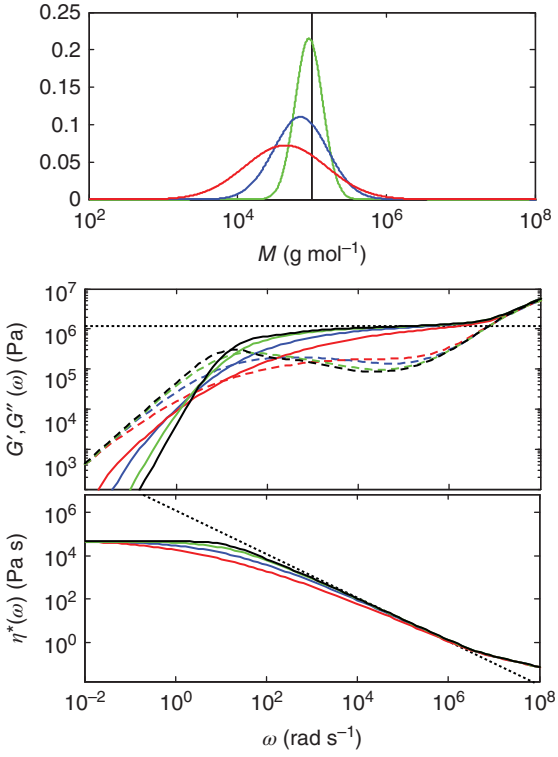

Figure 22 Illustration of the influence of polydispersity. The predicted curves correspond to 1,4-PBD with a molar mass distribution represented by a log-normal distribution with $M_w = 100$ kg mol^{-1} and a polydispersity of 1 (black), 1.2 (green), 2 (blue), or 5 (red).

chains depends on their molar mass (see Eqs. (19) and (20)), the viscoelastic data of polydisperse samples display a much broader spectrum of relaxation times, and the overall survival fraction of the initial tube at time t, $\varphi(t)$ (used in Eq. (26)), must include the contribution of each molar mass i at a fraction of v_i in the sample [54]:

$$\phi(t) = \sum_i v_i \phi_i(t). \tag{27}$$

The influence of (molar mass) polydispersity (PD) on the viscoelastic properties of linear chains is shown in Figure 22: by increasing PD, the low-frequency peak of the loss modulus becomes much broader, while the way the storage modulus decreases at low frequencies is much more gradual.

4.2 Linear Viscoelastic Properties of Star Polymers

Star polymers represent the simplest branched architecture. They contain only one branch point, which cannot easily diffuse since it is attached to several arms. As for linear chains, the relaxation of unentangled star polymer is well described by the Rouse model, while taking into account the extra friction coming from the branching point [55]. On the other hand, the relaxation of an entangled star polymer composed of arms of identical length is very different from the relaxation of a linear chain since the branching points prevent the arms from reptating. As illustrated in Figure 23 (black curves), star polymers relax much slower than the linear

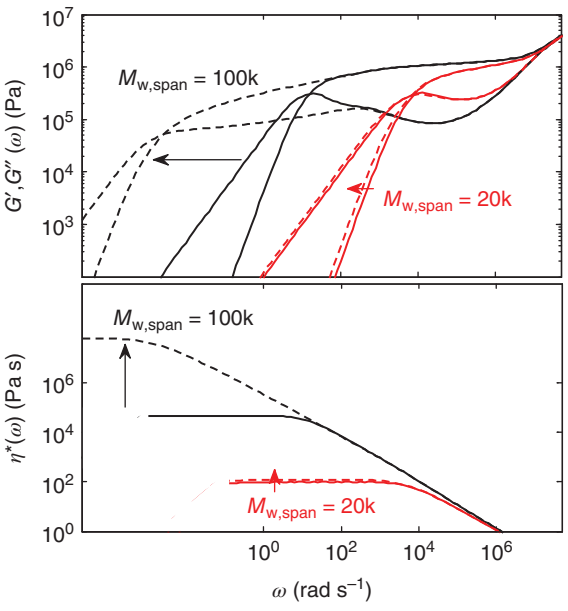

Figure 23 Viscoelastic response of monodisperse symmetric linear polymers (continuous curves) versus star chains (dashed curves) with same span molar mass of 100 kg mol^{-1} (black curves) and 20 kg mol^{-1} (red curves). The predictions have been obtained using the material parameters of 1,4-PBD and presented as frequency-dependent moduli (top) and complex viscosities (bottom).

chains of the same chemistry and with the same span molar mass, especially if they are well entangled [7, 29].

4.2.1 Relaxation of a Star Polymer

4.2.1.1 Relaxation of a Star Polymer in Comparison to a Linear Polymer

Several processes characterize the relaxation of a star polymer: (i) at very short times (or high frequencies), the star molecules relax their stress at a local level, through Rouse dynamics and LR. The stress relaxation modulus is therefore well described by Eq. (17). (ii) At times $t > \tau_e$, the star molecules reach their equilibrium state. Similarly to linear chains, the arm extremities can easily fluctuate (by CLF) and relax rapidly (see Eq. (20)). However, the CLF process stops for deeper arm segments, which feel the constraining effect of the entanglements. Thus, up to this point, the star molecules relax in the same way as the corresponding linear chains, as shown in Figure 23. (iii) At longer times, while reptation is observed for the linear chains, the star polymer rather shows a very slow and broad relaxation up to its terminal regime. This slow relaxation is attributed to another relaxation process, the arm retraction, which is described below. (iv) As in the case of linear chains, CR process occurs as soon as the star polymer disentangles (see Eq. (26)). As discussed below, CR also strongly influences the arm-retraction process.

4.2.1.2 Arm Retraction

The central molecular segments, which cannot reptate, can only relax by deep retraction within their tube [29]: as illustrated in Figure 24, when the arm contracts within its tube and then stretches out again, the orientation of the ends of the initial tube is forgotten, and the stress associated with those portions is

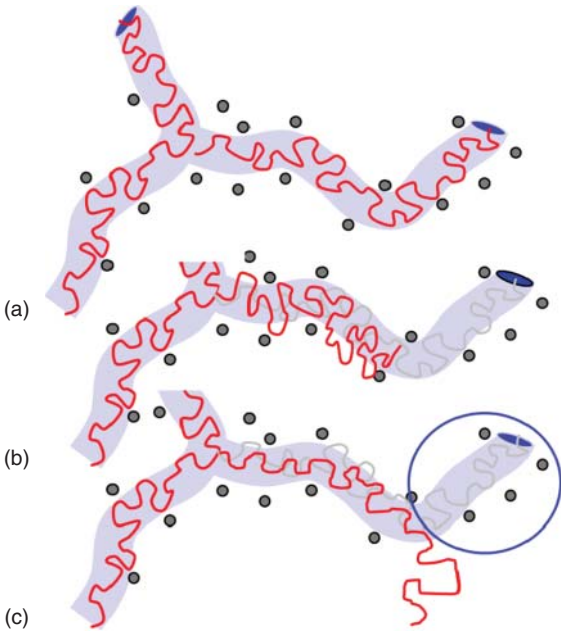

Figure 24 Illustration of the arm-retraction process, progressing with time from (a) to (c): (a) The length of the primitive path is equal to its equilibrium length, L_{eq}. (b) Arm-retraction process: the length of the primitive path is momentarily becoming shorter than L_{eq}. (c) When retracting to its equilibrium length, the arm does return to its initial configuration, and part of the initial tube is lost.

relaxed. These deep retractions arise because with time, the real length of the primitive path of an arm fluctuates around its equilibrium length L_{eq}, which represents the most probable length and which leads to the minimum value of the associated potential U/kT. If the real length of the primitive path becomes shorter than L_{eq}, the arm partially relaxes, as illustrated in Figure 24. Chain retraction is a typical first passage problem: as soon as the arm extremity fluctuates until a specific tube segment x_i, the memory of the orientation of the initial tube segment between $x = 0$ and $x = x_i$ is lost forever.

Since the retraction process is entropically unfavorable, the relaxation of the star arms takes very long time, which increases exponentially with the molecular weight of the arm, M_a, as well as with the depth of the molecular segment along this arm, from $x = 0$ at the extremity to $x = 1$ at the branching point:

$$\tau_{fluc}(x) = \tau_0(x) \exp\left(\frac{3M_a x^2}{2M_e}\right) \tag{28}$$

The exponential dependence of the relaxation time of an arm segment on its depth x explains why the star polymers, even if they are monodisperse and symmetric, are characterized by a very broad spectrum of relaxation times. Another important consequence is the large influence of DTD: since the outer segments of an arm relax much faster than the next, deeper segments, they can be considered as a solvent (through the rescaling of M_e in Eq. (28)) for the relaxation of the deeper segments [56]. Hence, the polymer fraction considered as solvent in the retraction process increases with the position of the segment (equivalently, with time). In fact, if this DTD effect was not taken into account when determining the relaxation time of an arm, the latter would easily reach relaxation times longer

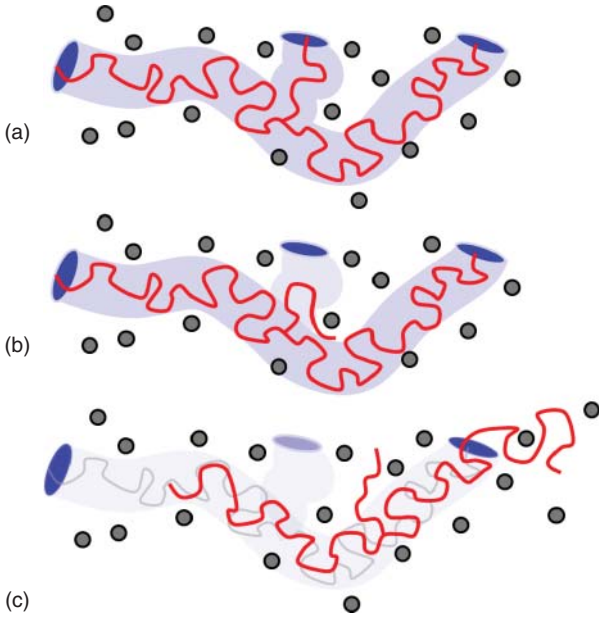

Figure 25 (a–c) Schematic illustration of the reptation process of an asymmetric star polymer composed of two long and a short arms. The center of mass of the molecule can diffuse, at the rhythm of the motion of the short arm.

than 10^{20} s. Finally, an important message from Eq. (28) is that the relaxation of the star does not depend on the number of arms.

4.2.1.3 Reptation of an Asymmetric Star Macromolecule

While a symmetric star polymer cannot reptate, it is possible for an asymmetric star molecule, which contains only two long arms in addition to one or more short arms, to partially relax via reptation, after the short arms have relaxed [57]. In such a case, as illustrated in Figure 25, the branch point can only diffuse at the rhythm of the breathing of the short arm. On average, one can consider that the time necessary for the branch point to diffuse a distance of one entanglement segment is proportional to the retraction time of the short arm. The latter can be thought of as additional friction that the chain backbone (defined by the span length, i.e. two long arms) must overcome in order to diffuse, and which must be added to the friction coming from the backbone (span length) of the star molecule. Consequently, with well-entangled arms the diffusion coefficient (see Eq. (18)) and the effective reptation time (see Eq. (19)) of the star molecule can be much larger than those of a respective linear polymer with same span length [57, 58].

It should be noted, however, that besides introducing additional friction to the diffusion of the asymmetric star's "backbone" (span length comprising the two large arms, see Figure 25), short arms also amplify the CR effect [29]. These two opposite effects acting on the relaxation of the backbone are further discussed in Section 4.3.2 with comb architectures.

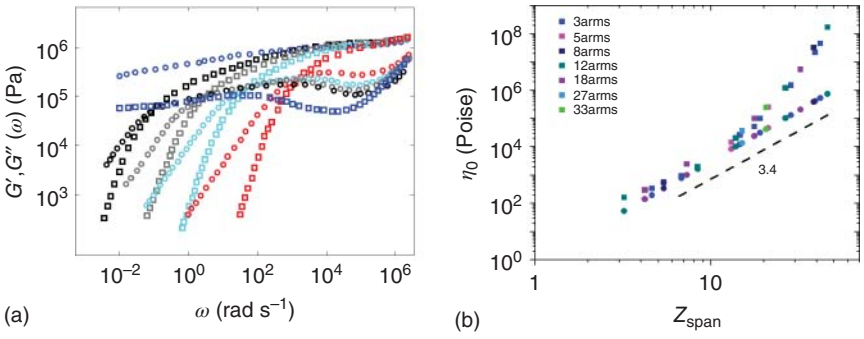

Figure 26 (a) Viscoelastic moduli of monodisperse symmetric star polybutadiene with 4 arms of molar mass of 10.7 kg mol^{-1} (red), 20 kg mol^{-1} (cyan), 28.7 kg mol^{-1} (gray), 38.5 kg mol^{-1} (black), and 93.8 kg mol^{-1} (blue) [59]. Source: Based on J. Roovers, Properties of the plateau zone of starbranched polybutadienes and polystyrenes, Polymer 26, 1091–1095 (1985). (b) Zero-shear viscosity versus span molar mass for symmetric star polymers (□) of varying span (2 arms) number of entanglements and arm number, along with the respective data for linear chains (o) [60]. Source: Data from L. J. Fetters, A. D. Kiss, D. S. Pearson, G. F. Quack, F. J. Vitus, Rheological Behavior of Star-Shaped Polymers, Macromolecules, 27, 647–654 (1993).

4.2.1.4 Influence of the Molecular Characteristics on the Dynamics of Star Polymers

4.2.1.4.1 Influence of the Arm Molar Mass The retraction time of an arm increases exponentially with the number of its entanglements (see Eq. (28)). Therefore, as illustrated in Figure 26a, the influence of M_a is very large.

The exponential increase in the zero-shear viscosity of monodisperse stars as a function of the number of entanglements per arm is shown in Figure 26b. For comparison, the viscosity of the linear chains is also shown. As is evident from this figure and has been already mentioned, the difference in dynamics between star and linear polymers becomes significant when the number of entanglements increases (see Sections 4.1.2.3 and 4.2.1.2).

4.2.1.4.2 Influence of the Number of Arms In Figure 26b, we can also observe that the viscosity does not depend on the number of arms of the star molecule. This observation is valid as long as the volume occupied by the branching point is negligible compared to the volume occupied by the arms. Indeed, if a star polymer contains a large number of arms (functionality typically above 32), the arm segments close to the branching point form an effective core, and the multiarm star polymer behaves similarly to core–shell particles, exhibiting an extra relaxation in its viscoelastic response, due to the slow relaxation of the cores [61]. Remarkably, due to the fact that the viscosity of low-functionality stars does not depend on the number of arms but rather on the length of one arm, star polymers can have a very large total molar mass but with a very low viscosity compared to their linear counterparts. Similar properties can also be found with hyperbranched architectures.

4.2.1.4.3 Influence of Polydispersity (PD) This is illustrated in Figure 27. Compared to linear polymers with molar mass equal to their span molar mass (Figure 23), stars are characterized by a much more pronounced influence of

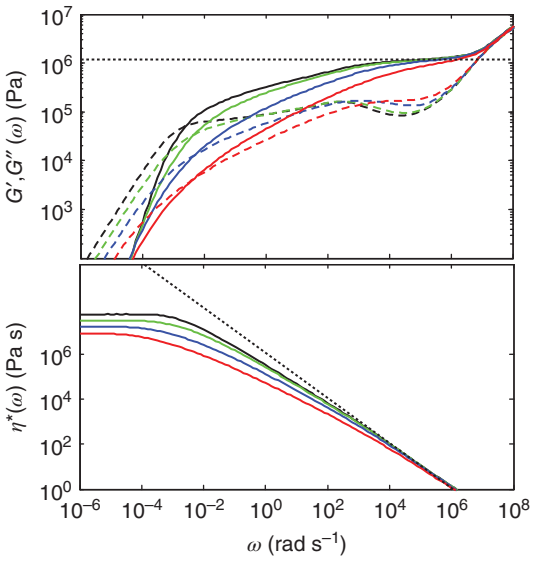

Figure 27 Illustration of the influence of polydispersity. The predicted curves correspond to a 1,4-PBD star with $M_{w,arm} = 50$ kg mol^{-1} and with an arm polydispersity of 1 (black), 1.2 (green), 2 (blue), or 5 (red). Top plot represents frequency-dependent moduli and bottom the respective complex viscosities.

PD on the zero-shear viscosity. This is due to its exponential dependence on the arm molar mass and the large dilution effect of the shorter arms on the retraction process of the longer ones. PD affects both the zero-shear viscosity and the overall shape of the complex viscosity curves. Similarly, if a star polymer is diluted in a short linear matrix, its relaxation will speed up more profoundly compared to a long linear polymer under the same conditions. This is due to the fact that DTD influences the retraction process exponentially.

4.3 Linear Viscoelastic Properties of Branched Polymers

4.3.1 Relaxation of the Inner Generations of Branches

The linear viscoelastic response of complex macromolecular architectures results from a combination of different relaxation mechanisms based on linear (two ends of a segment free) and star (only one end free) relaxations. At short times, the molecules relax first at local scale through Rouse dynamics. Then, the outer generation of branches will relax in a similar way as the relaxation of the arms of a star molecule, i.e. by CLF and arm retraction (see Section 4.2). CR mechanisms must also be taken into account. The main difference between the relaxation of a star molecule and the one of a complex architecture is the very slow relaxation of the polymer fraction which is trapped between two branching points. Indeed, the inner branches cannot relax before the branching points release their stress, an action that can only take place after the outer branches have relaxed. Therefore, their relaxation times are necessarily much longer than those of the outer generations of branches (located closer to the extremities of the molecule). This leads to the important concept of *hierarchical motion*, according to which the outer generation of branches relaxes first, followed by the relaxation of the inner branches [4, 7, 9, 29]. This hierarchical relaxation is illustrated in Figure 28, which shows the storage and loss moduli of a model "pom-pom" polymer: While the

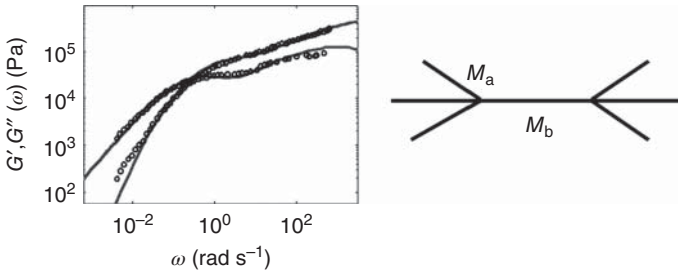

Figure 28 Storage and loss moduli of 1,4-PBD pom-pom having molar mass of an arm 14.8 kg mol^{-1} and molar mass of the inner backbone 47 kg mol^{-1}. Since the inner part of the backbone is trapped between two branching points, its relaxation can only take place at low frequency. Symbols represent the experimental data [62], while the continuous curves represent the predictions based on a tube model (see text). Source: E. Van Ruymbeke, C Bailly, R. Keunings, and D. Vlassopoulos, A general methodology to predict the linear rheology of branched polymers, Macromolecules 39 (18), 6248–6259, https://doi.org/10.1021/ma0604385.

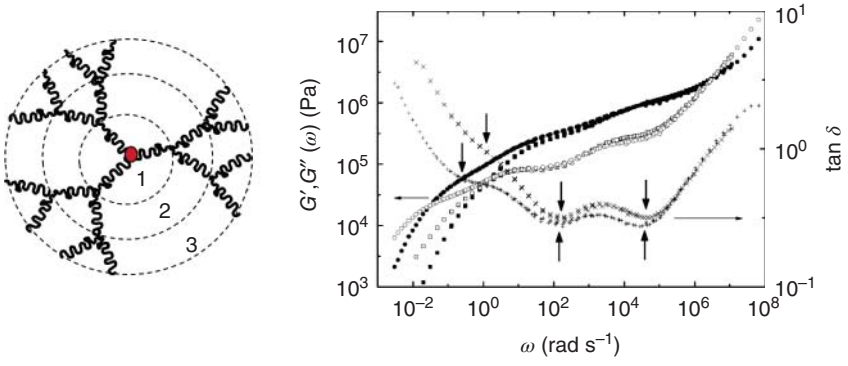

Figure 29 Viscoelastic properties (moduli and tangent of loss angle or phase angle, indicated by horizontal arrows) of symmetric Cayley-tree 1,4-PBD with three generations of branches. The molar masses of the different generations (from outer to inner) are 5, 6, and 32 kg mol^{-1} (o, +) or 5, 6, and 5 kg mol^{-1} (□, x) [63]. Source: E. van Ruymbeke, K. Orfanou, M. Kapnistos, H. Iatrou, M. Pitsikalis, N. Hadjichristidis, D. J. Lohse and D. Vlassopoulos, Entangled dendritic polymers and beyond: Rheology of symmetric Cayley-tree polymers and macromolecular self-assemblies, Macromolecules, 40, 5941–5952, https://doi.org/10.1021/ma0706024.

outer branches relax at relatively high frequencies (around 100 rad s^{-1}), a second plateau appears in the storage modulus at low frequencies (around 1 rad s^{-1}), between the relaxation of the outer branches and the very slow relaxation of the inner backbone, moving at the rhythm of the motions of the branching points.

Another example is shown in Figure 29 for a monodisperse Cayley-tree polymer with three generations of branches. In such a case, the viscoelastic moduli show three successive relaxation modes corresponding to the three generations of branches.

While the inner generations of branches relax by reptation or retraction, the extra friction originating from the branching points must be included in these

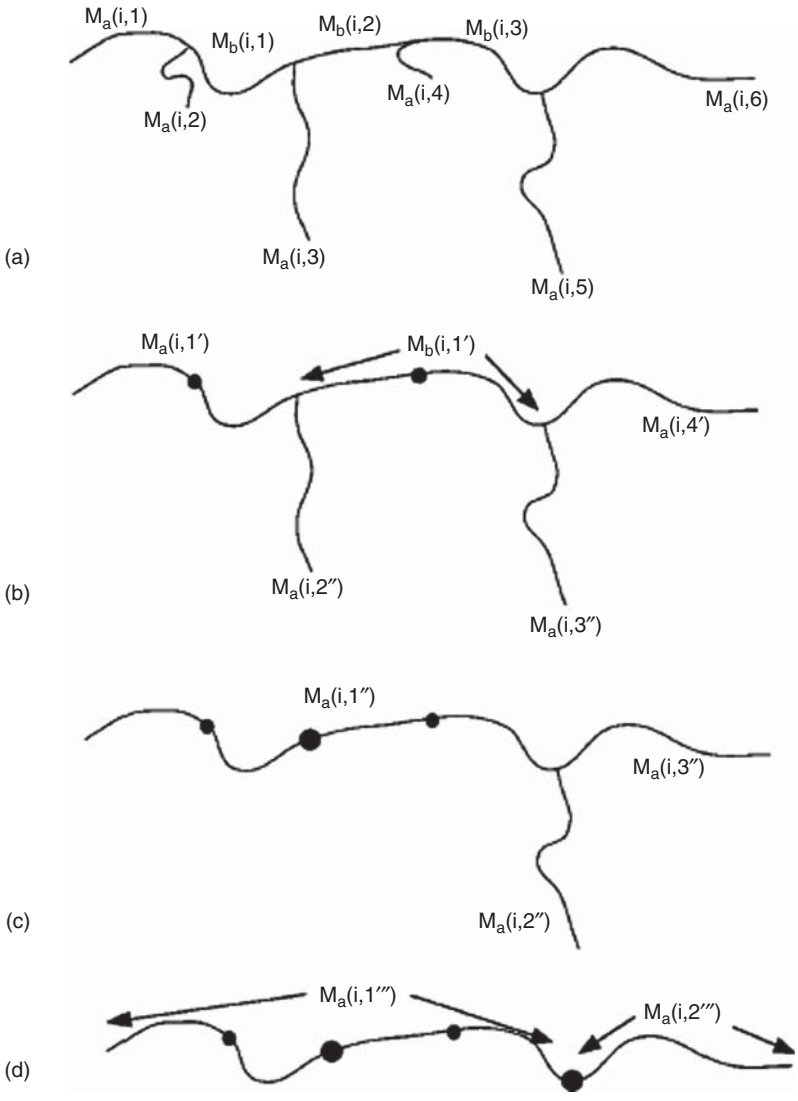

Figure 30 (a–d) Schematic illustration of the hierarchical relaxation of a branched macromolecule. After the imposed deformation, only the branches (with one free end) can move by retraction. When a branch with a given molar mass fully relaxes, it is replaced by an effective bead at the branching point, to take into account the frictional drag of the branch [64]. Source: R. G. Larson, Combinatorial rheology of branched polymer melts, Macromolecules, 34(13), 4556–4571, https://doi.org/10.1021/ma000700o.

processes, as illustrated in Figure 30: as soon as a branch has relaxed, it acts as an extra friction point, whose importance depends on the relaxation time of the relaxed branch. It can strongly slow down the diffusion of the inner molecular segments.

4.3.2 Constraint Release in Branched Polymers

Similarly to linear and star polymers, the CR process is present during relaxation of branched polymers. With model architectures such as monodisperse H, pom-pom, and comb polymers, the dilution effect of the outer branches on the inner segments can easily be detected since the outer branches are relaxing before the inner branches and can therefore be considered as solvent for the relaxation of the inner backbone [29, 63, 64]. As already mentioned, this leads to the appearance of a second, low-frequency plateau modulus, observed after the relaxation of the outer branches (Figures 28 and 29). Like in Eq. (22), the level of this second plateau, G_2, depends on the fraction of polymer segments trapped between two branching points, $\upsilon_{\text{inner generations}}$, as

$$G_2 = G_0^N \, \upsilon_{\text{inner generations}}{}^{1+\alpha} \tag{29}$$

Thus, the larger the fraction of dangling branches, the lower the level of this second plateau will be [28].

4.3.3 Influence of Molecular Characteristics of Branched Polymers on Their Dynamics

4.3.3.1 Influence of the Length of the Branches

If the outer branches of a complex macromolecule are long, the friction they impart on the backbone is large, and consequently, the inner segments need longer time to relax. This is illustrated in Figure 31, which compares the viscoelastic properties of model comb polymers with the same backbone, similar number of branches (around 30), but different lengths of the branches. It is observed that increasing the length of the branches delays their retraction time, as expected from Eq. (28). But it also leads to the development of a second relaxation mode at low frequencies, due to the increase in the backbone relaxation time and the enhanced dilution effect of the outer branches (see Eq. (29)). There is a clear interplay between the two modes (branch and backbone) due to the opposite effects of enhanced friction and enhanced dilution.

4.3.3.2 Influence of the Number of Outer Branches

As already mentioned, the dilution effect of the branches speeds up reptation and retraction processes of the inner branches, in contrast to the extra friction they impart. Depending on their number as well as their length, one of the two effects will dominate, leading to either an overall speedup or slowing down of the relaxation of the inner branches. This is illustrated in Figure 32, which compares two comb architectures with the same backbone length and similar total fraction of branches [65]. It is seen that the comb polymer composed of many short branches relaxes much faster than the respective linear polymer with molar mass equal to that of the comb backbone. In the latter case, the dominant effect from the branches is its dilution effect. On the other hand, the relaxation of a comb polymer composed of fewer but longer branches is much longer than that of the respective linear polymer. Hence, in this case, it is the friction of the branches that controls the relaxation of the comb backbone. Usually, speedup of the relaxation process is observed if the branches are unentangled.

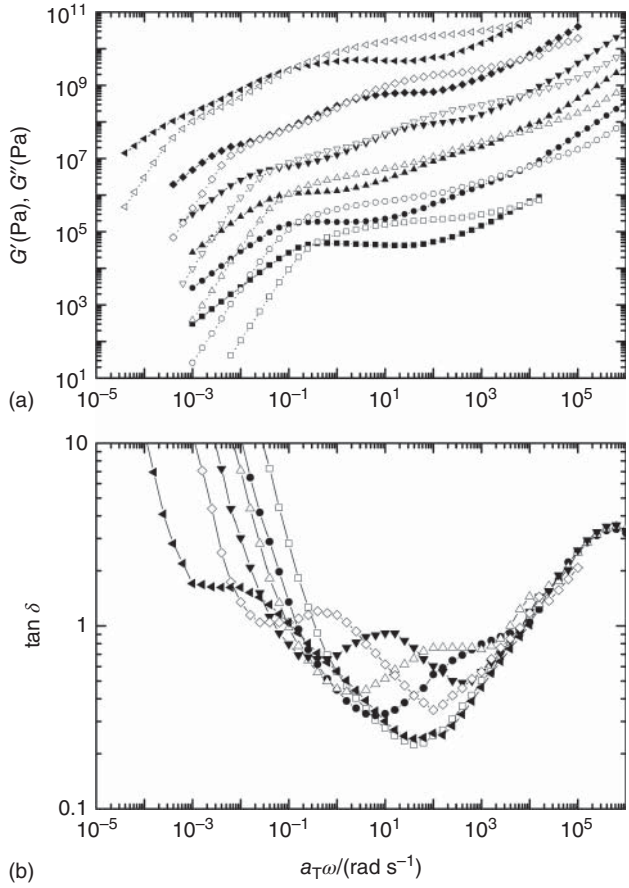

Figure 31 (a) Storage and loss moduli and (b) tanδ (tangent of the loss factor or phase angle) curves of polystyrene comb-like polymers. The molar mass of the backbone is 275 kg mol^{-1}. Each polymer has around 30 branches, each with molar mass (from bottom up in a) of 6.5, 11.7, 25.7, 47, and 98 kg mol^{-1}. In (a), the moduli have been vertically shifted by factors of 1, 10, 10^2, 10^3, 10^4, and 10^5 for clarity [28]. Source: M. Kapnistos, D. Vlassopoulos, J. Roovers and L. G. Leal, Linear rheology of architecturally complex macromolecules: Comb polymers with linear backbones, Macromolecules, 38, 7852–7862, https://doi.org/10.1021/ma050644x.

4.3.3.3 Influence of Polydispersity

4.3.3.3.1 Polydispersity in Model Architectures While it is not easy to highlight the influence of PD based on model branched architectures, its effect is important, especially if it is related to the PD of the outer generation of branches. However, molecular segments of model architectures are usually synthesized via anionic polymerization and have a very low molar mass PD. Several works in the literature have shown that the main challenge with these model complex architectures is not handling the influence of molar mass dispersity but rather the possible architectural PD of the polymer, i.e. the possible presence of different molecular structures [66]. Indeed, given the very complex synthetic procedure,

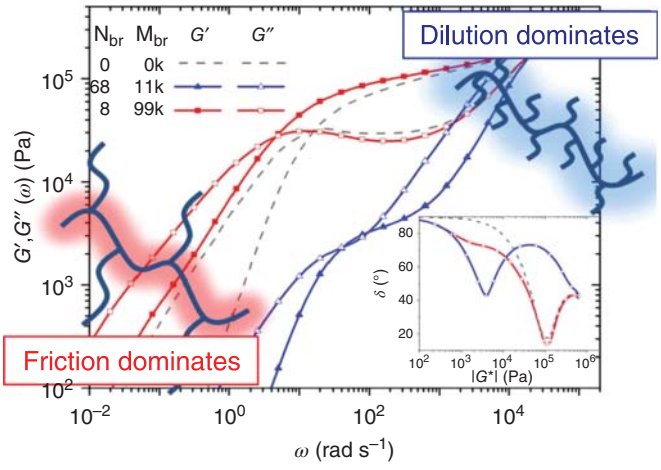

Figure 32 Predicted frequency-dependent linear viscoelastic properties (moduli in main plot and tangent of loss factor in inset) for poly-*n*-butyl acrylate (PnBA) comb polymers composed of a backbone of 140 kg mol^{-1}, with 8 branches of mass 99 kg mol^{-1} (red □), 38 branches of mass 11 kg mol^{-1} (blue Δ), or without branches (gray --) [65]. Source: Modified from M. Ahmadi, S. Pioge, C.A. Fustin, J.F. Gohy, and E. van Ruymbeke, Closer insight in the structure of moderate to densely branched comb polymers by combining modelling and linear rheological measurements, Soft Matter, 13, 1063–1073 (2017).

the presence of side products such as incomplete branched macromolecules is almost unavoidable and can significantly affect the final viscoelastic properties. A way to overcome this issue is to fractionate the polymer, for example by Temperature Gradient Interaction Chromatography [55, 66].

4.3.3.3.2 Polydispersity in Randomly Branched Polymers While model polymers are of prime importance in order to understand the relaxation mechanisms in complex architectures, most of the branched polymers contain a large variety of branched architectures, and their exact compositions are usually unknown. Depending on the polymerization protocol, information from the sample synthesis can be coupled with specific statistical tools in order to determine the most probable composition of the branched polymer, which can then be used in order to determine their viscoelastic behavior [66, 67].

Statistical approaches are particularly efficient for describing the composition of branched polydisperse polymers that follow classical Monte Carlo statistics, as for example, polycarbonate, polyesters, polyamides, and polyurethane samples. It has been shown that with such polymers the molar mass distribution (MMD) of any molecular strand between two chain ends/branching points is well described by a Flory-type MMD with the same number average molar mass, $M_{n\,\mathrm{strand}}$. Therefore, if the different chemical components are known, the only unknown needed to determine their statistical MMD is the conversion level. Its value can be determined via best-fitting procedure by comparing the theoretical MMD and the experimental SEC/LS curve. It is thus possible to determine the most probable composition from the SEC/LS curves and then use it for predicting the viscoelastic data of the sample [67, 68]. As illustrated in Figure 33

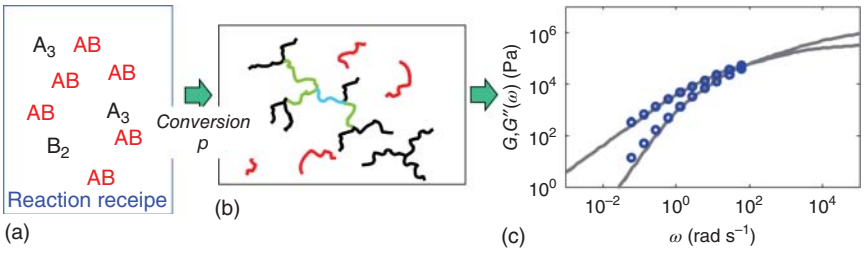

Figure 33 (a) Example of a statistical composition of a branched polyamide 6 composed of caprolactam (AB) as monomer, Tris-caproic acid melamine (A_3) as branching points, and hexamethylene diamine (B_2) as chain extender, at specific ratios. (b) Decomposition of the macromolecules into generations of branches of the same distance from the chain extremity, measured as number or generations (represented by the different colors), used for predicting the frequency-dependent viscoelastic moduli (c) [68].

for a branched polyamide 6 sample, the latter step, which is a priori complex due to the large variety of macromolecules, can be substantially simplified if one models the relaxation of all molecular strands by considering groups of strands having the same distance from the chain extremity, measured as number or generations [68], rather than by considering each architecture separately.

However, in other cases, for example low density polyethylene (LDPE), determining the statistical composition remains a big challenge. Note that Tobita [69] developed an algorithm based on the Monte Carlo scheme from free radical polymerization of ethylene to polyethylene, taking into account the reaction schemes such as initiation, propagation, scission, branching, and different processes of termination.

4.3.3.4 Modeling the LVE of Branched Polymers

The viscoelastic properties of branched polymers have been described by several tube models, such as the Branch-on-Branch (BoB) model [4, 70, 71], the hierarchical model [64], and the Time Marching Algorithm (TMA) model [62]. These approaches have been validated for model branched polymers, in particular pom-pom [62, 72, 73], comb [28, 74, 75], or Cayley-tree architectures [63, 76]. While the models differ in the way the relaxation processes are implemented [73], they are all based on the hierarchical concept introduced in Section 4.3.1 [64]: after the relaxation of the outer generation of branches, which are relaxing in a way similar to that of the arms of a star molecule, the reptation and fluctuation processes of the molecular segments trapped between two branching points can take place. Their corresponding relaxation times are determined by accounting for the extra friction coming from the branches attached to the inner segment. In the models, this extra friction is calculated based on the assumption that the relaxation time of a branch corresponds to the time needed for the branching point on which the branch is attached to diffuse along a distance equal to the distance between two entanglements, a, or a fraction, p, of this distance [57]. The typical values used for p^2 are 1/12 [73], 1/40 [70], or 1 [62]. When several branches are attached to a branching point, the total friction associated with

it is considered as equal to the sum of the frictions determined for each of the branches [64]. The extension of these models to polydisperse branched samples has been proposed in Refs. [65–68, 71, 72]. For such complex systems, the polymer fraction relaxed at a specific time t cannot be determined analytically. Therefore, it is determined step by step through time, based on the relaxation times of the molecular segments. The values of the latter also vary and therefore must be updated at each time step, as function of the polymer relaxed at the previous time step. Based on such an approach, the BoB model combined with a Monte Carlo algorithm to determine the most probable composition, has been very successful in describing the linear viscoelastic properties of LDPE samples [70, 71].

5 Nonlinear Viscoelasticity

In industrial polymer processes, polymers are subjected to a combination of nonlinear shear and extensional flows. In general, these flows can be classified by the relative amount of stretch versus rotation: rotational flows are relatively weak, whereas stretching flows are stronger and may deform the microstructure of the chain.

Shear flow is a combination of (mild) stretch and rotational flow. While the stretch component causes polymer chains to orient in the direction of flow and deform, the rotational component forces them to tumble; hence, it suppresses their stretch (Figure 34a). On the other hand, uniaxial extensional flow is a purely (strong) stretching flow and can lead to highly stretched polymer chains, as represented in Figure 34b. As illustrated in Figure 3, because of these differences at the molecular level, the viscoelastic response of an entangled polymer under shear or under elongation flow differs substantially [12].

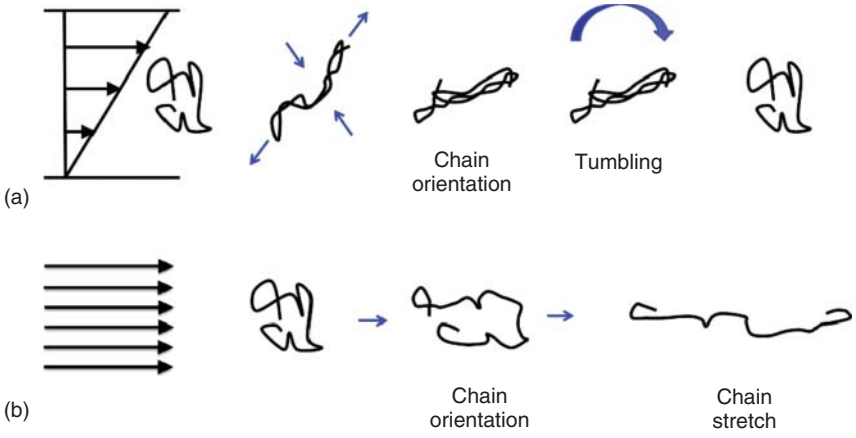

Figure 34 Schematic illustration of conformation changes of polymeric coils undergoing shear (a) and extensional (b) flow.

5.1 Nonlinear Shear Rheology

5.1.1 Shear Thinning of Linear and Branched Polymers: Steady-State Predictions and Measurements

Under nonlinear shear flow, entangled polymer melts exhibit shear thinning (Figure 3c and d). This decrease in steady viscosity observed at large values of the shear rate can be attributed to the flow-induced partial disentanglement of the polymer. However, the exact conformational properties of the macromolecules in the thinning regime as well as the exact value of the corresponding thinning slope are not yet fully understood [8, 9]. A first approach to rationalize shear thinning is by means of the empirical Cox–Merz rule, which states that $\eta(\dot{\gamma}) = \eta^*(\omega)$ when $\dot{\gamma} = \omega$, or equivalently $\eta(\mathrm{Wi}) = \eta^*(De)$ [77]. This equivalence was not expected a priori, since the steady viscosity $\eta(\dot{\gamma})$ is measured in the nonlinear regime under nonequilibrium conditions, whereas $\eta^*(\omega)$ is measured in the linear regime under small amplitude oscillatory shear (equilibrium). The meaning of this rule is that at high rates only the fast modes (i.e. local modes excited by the applied rate) of the polymers contribute to its viscosity since slower modes have not yet had time to relax and contribute to energy dissipation. This rule, which also implies an equivalence between shear stress and complex modulus [78], has been validated for linear (Figure 35a) and star polymers [80], although a small differentiation of steady shear from dynamic viscosities is observed at high rates, possibly due to wall slip which results in lower values of the former [10]. In general, the Cox–Merz rule fails for branched polymers (Figure 35b) [79]. Rabin and Öttinger developed a scaling model [81] for shear thinning in good and theta solvents, which, however, applies to melts as well. They considered the polymeric chain to comprise shear blobs, i.e. sections with relaxation time $\tau = \dot{\gamma}^{-1}$ that relax at a given shear rate $\dot{\gamma}$. Larger polymer sections are deformed by the shear flow because they do not have time to relax. Hence, the effect of shear deformation is screened at the blob size. For unentangled melts, Colby and coworkers have accounted for the change

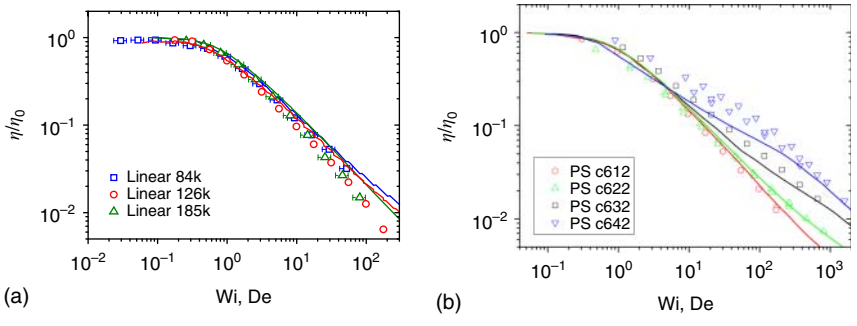

Figure 35 (a) Application of Cox–Merz rule for linear polystyrenes for molar masses 84, 126, and 185 kg mol^{-1}. Symbols and solid lines refer to shear and dynamic measurements, respectively. (b) Respective data for comb polystyrenes with the same linear backbone molar mass of 275 kg mol^{-1} (code c6), the same number of branches [29], and increasing molar mass of branch (12, 22, 32, and 42 kg mol^{-1}). The Weissenberg number is based on the terminal time [79]. Source: Based on F. Snijkers and D. Vlassopoulos, Appraisal of the Cox-Merz rule for well-characterized entangled linear and branched polymers, Rheol. Acta, 53: 935–946 (2014).

in conformation of a polymer under shear flow by considering the deformed chain as a train of tension blobs that behave elastically while exhibiting ideal chain statistics and reduced energy dissipation (via reduced blob size) as the shear rate increases [82]. The resulting shear thinning exponent of −1/2 was found to be in good agreement with the available data on unentangled polymer melts [82–84]. In this analysis, the onset of shear thinning occurs at a terminal Weissenberg number (based on the terminal time of the polymer) $\mathrm{Wi}_t = 1$ [82]. However, recent nonequilibrium molecular dynamics (NEMD) simulations with unentangled melts suggest that shear thinning starts at larger values of Wi_t (which depend on the degree of polymerization), when a substantial fraction of chains are stretched [85], because chain size reduction is appreciable only when the chains are nonlinearly stretched; this occurs at a Rouse Weissenberg number $\mathrm{Wi}_R \geq 1$. Another extensive NEMD simulations study with melts of varying chain lengths [86] suggests that shear thinning starts at $\mathrm{Wi}_t = 1$ and is characterized by two regimes, a first with slope of −0.45 for unentangled chains, and a second at higher shear rates (likely associated with saturated stretch of the chains) with a weaker, universal (for all chain lengths) thinning slope of −0.37. This second regime is also reported in other NEMD simulations, albeit with different slope (−0.44) and entangled chains [87]. In the spirit of chain deformation, an alternative theoretical approach by Subbotin et al. [88] accounted for finite chain extensibility in unentangled melts with friction force acting only in the direction of flow, yielding a thinning slope of −2/3. Note for completion that a common approach to introduce thinning to unentangled chains (which do not shear-thin according to Rouse model) is by means of finite extensibility, the so-called FENE model [89, 90]. The message from the above is that, while shear thinning can be accounted for, a full molecular picture is still lacking.

Entangled chains also shear thin at $\mathrm{Wi}_t \geq 1$. The Doi–Edwards tube model predicts an instability in this regime, which is prevented by incorporating the convective constraint release (CCR) mechanism [91]. The latter suggests that at the onset of nonlinearity the characteristic rate of the material under flow is its thermal (terminal) rate augmented by the imposed shear rate. The physical picture is that at $\mathrm{Wi}_t = 1$ chains start orienting, and at Rouse Weissenberg number $\mathrm{Wi}_R = 1$ they start stretching. Tube modeling based on CCR involves parameters describing the amount of CCR, nonaffinity, partial loss of entanglements, and finite extensibility. Depending on their choice, the regime between orientation and saturation of stretch can be tuned; hence, the thinning slope is not universal [92, 93]. CCR is included in GLaMM, a differential constitutive model that incorporates thermal CR as well [94]. In addition, transient tumbling is expected to take place after chain segments are convectively disengaged [95], whereas at very high rates in the strong stretching regime the monomeric friction is expected to be anisotropic albeit system dependent [96] and the thinning slope weaker [86]. The latter regime should be observed at rates beyond τ_e^{-1}. A tube model including CCR, tumbling, and anisotropic friction seems to capture the transient and steady response of entangled polymers, though the rates were apparently not high enough to reach the second thinning regime, and accordingly, the anisotropic friction effects were minimal [12]. Experiments with entangled nearly monodisperse polymer melts reveal shear thinning weaker than −1, with a slope of about −0.82 [12, 97]. Concerning the high-rate regime with reduced thinning slope,

simulations do not yet converge to a universal value [86, 87], yet the apparent independence on N reported in experimental studies [98] conforms to a saturated stretch picture. Note that in experimental results the PD is an issue since it affects the thinning slope [98]. Some very recent developments have addressed the transient shear response (overshoot and undershoot) and steady shear thinning behavior by means of modeling and simulations [99–101].

As discussed in Section 2, rheological measurements of fast shear flows of polymers are very challenging because of the occurrence of instabilities at large values of the imposed shear rate $\dot{\gamma}$, and the use of a CPP geometry is needed in order to obtain reliable data with rotational geometry [11–14, 102].

5.1.2 Transient Nonlinear Response of Linear and Branched Polymers

For entangled polymers, the start-up of shear flow is typically associated with a rich response characterized by a stress overshoot, followed by an undershoot and eventually a steady state (Figure 36a). The overshoot is associated with orientation (when the shear rate exceeds the inverse terminal time but is below the inverse Rouse time) and stretching (at rates above the inverse Rouse time) of chain segments [12, 103] and can be quite complex (double overshoot) for branched polymers (Figure 36b) or polymer blends due to the interplay of two time scales, associated with branch and backbone or long and short component, respectively [104]. The observed undershoot has been recently assigned to tumbling of the entangled polymers following their viscosity peak, i.e. maximum instantaneous deformation in flow [12, 99], but more work is needed, both experimentally

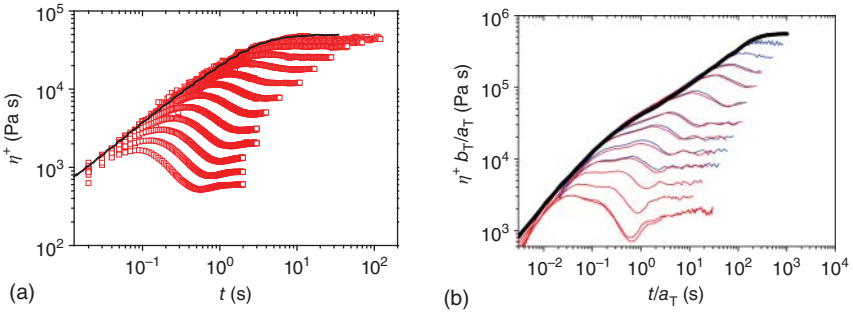

Figure 36 Start-up shear flow: Transient viscosity (shear stress growth coefficient) versus time measured at different shear rates for (a) entangled linear polystyrene of 285 kg mol^{-1} dissolved in oligomer 2 kg mol^{-1} at concentration of 47%, different shear rates from 0.1 s^{-1} (top) to 100 s^{-1}, with the solid line being the linear viscoelastic envelope, extracted from the dynamic oscillatory measurements [12] and (b) entangled comb polystyrene with backbone molar mass of 275 kg mol^{-1} and 30 branches, each of 42 kg mol^{-1} [104]. The blue lines are obtained at 169.5 °C (at rates from 0.01 to 17.8 s^{-1}, from top to bottom) and the red lines at 160 °C (from 0.03 to 31.6 s^{-1}) and shifted to 169.5 °C (resulting in the range of rates from 0.1 to 105 s^{-1}). The black line is the linear viscoelastic envelope. Source: (a) S. Costanzo, Q. Huang, G. Ianniruberto, G. Marrucci, O. Hassager and D. Vlassopoulos, Shear and Extensional Rheology of Polystyrene Melts and Solutions with the Same Number of Entanglements, Macromolecules 49, 3925–3935, https://doi.org/10.1021/acs.macromol.6b00409. (b) F. Snijkers, D. Vlassopoulos, G. Ianniruberto, G. Marrucci, H. Lee, J. Yang, and T. Chang, Double stress overshoot in start-up of simple shear flow of entangled comb polymers, ACS Macro Lett. 2, 601–604, https://doi.org/10.1021/mz400236z.

and theoretically, to uncover all features of this interesting phenomenon. The situation with transient shear response is not fully resolved for unentangled polymers [105, 106], although simulations and experiments with star polymers [107] suggest a qualitatively similar behavior, due to the finite extensibility of the arms. However, important open issues associated to the transient viscosity peaks remain [108]. Note in passing that relaxation upon cessation of steady shear flow contains interesting information. Typically, it comprises two modes for high shear rates, a faster associated with the relaxation of the fast modes of the orientation spectrum and a slower, which is linked to terminal relaxation [12, 109]. The fast relaxation depends on shear rate, unlike the slow one. This relaxation is more evident in branched polymers, e.g. combs and stars for a range of shear rates, and can be considered as a characteristic feature of these polymers [80, 109].

5.2 Nonlinear Extensional Rheology

5.2.1 Monodisperse Linear Polymers

Figure 37a depicts the rate-dependent steady elongational viscosity along with the steady shear viscosity multiplied for the Trouton ratio [3] for monodisperse linear polymer melts. It is clear that the application of the Cox–Merz rule to uniaxial extension does not work: it has been observed that the steady shear viscosity and the dynamic viscosity of linear polymer melts (Figure 6d) exhibit much stronger thinning with almost double slope exponent compared to the $-1/2$ exponent observed with their steady elongational viscosity [110, 111]. As illustrated in Figure 3e and f, this weaker thinning is accompanied by a transient hardening of the chains, observed at elongation rates larger than the inverse Rouse time of the chains and attributed to partial stretching of the chains before their disentanglement. While this weak thinning regime has been observed in all monodisperse well-entangled linear polymer melts investigated, in poorly entangled linear polymer melts it is preceded by a short viscosity increase regime (extension-rate thickening), which takes place just after the linear regime of viscosity (Figure 37a). For completeness and to avoid misinterpretation, it is important to note that while the majority of published works with model entangled linear polymers are with polystyrene and indeed show extension-rate thinning (weaker than shear-rate thinning), recent data with polyisoprene and poly(*n*-butyl acrylate) show thickening at the highest extensional rates achieved [112] (Figure 3e and f). Hence, the behavior is not entirely understood yet and likely not universal. Another important finding refers to entangled polymer solutions, whose evolution of the elongational steady viscosity as a function of the Hencky strain rate is very different [113–117]: the steady viscosity at rates exceeding the inverse Rouse time of the chains increases substantially with the Hencky strain rate, leading to remarkable extension-rate thickening. Eventually, as illustrated in Figure 37b, this thickening regime is followed by an elongational thinning regime with a characteristic slope of $-1/2$ at very high extension rate.

The difference between the elongational properties of melt and solution has been extensively studied in recent years by Hassager and coworkers [115–117]. However, its origin is not yet fully elucidated. The elongational thinning of melts with a power-law scaling of $\eta_E \sim \dot{\varepsilon}^{-1/2}$ is not predicted by the Doi–Edwards

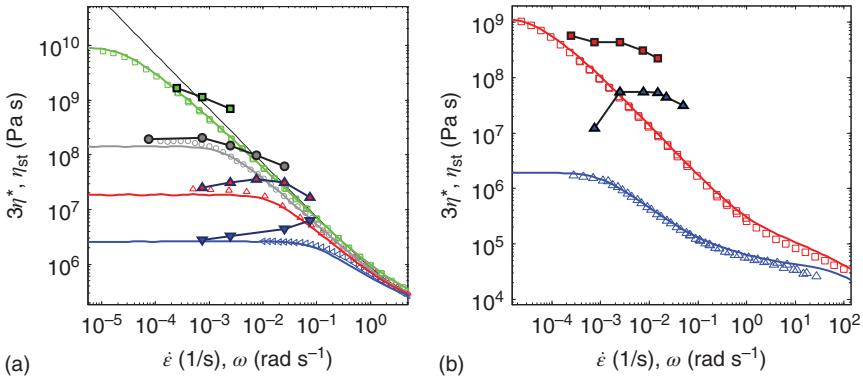

Figure 37 Complex viscosity (multiplied by 3, the Trouton ratio) (open symbols) and steady elongational viscosity (filled symbols) of (a) a monodisperse linear polystyrene with molar mass 545 kg mol^{-1} (green), 185 kg mol^{-1} (gray), 103 kg mol^{-1} (red), and 50 kg mol^{-1} (blue) in the melt state [108] and (b) a monodisperse linear polystyrene with 820 kg mol^{-1} diluted at 50 wt% (red) or at 10 wt% (blue) in styrene oligomers of 8.8 kg mol^{-1} [45]. Source: (a) Data from P. G. Santagelo and C. M. Roland, Interrupted shear flow of unentangled polystyrene melts, J. Rheol. 45, 583–594 (2001). (b) Data from T. Shahid, Q. Huang, F. Oosterlinck, C. Clasen, and E. van Ruymbeke, Dynamic dilution exponent in monodisperse entangled polymer solutions, Soft Matter, 13 (1) 269 (2017).

model [3]. Instead, this model predicts a behavior similar to that of linear polymer solutions, i.e. orientation and stress saturation at rates exceeding the inverse reptation time, with a slope of −1 and then a strong increase in stress at rates exceeding the inverse Rouse time [118]. In order to explain the elongational thinning of melts, anisotropic friction with finite chain extensibility has been invoked, an idea that has been supported by simulations [96, 119, 120].

5.2.2 Polydisperse Linear Polymers

PD strongly affects the elongational properties of linear polymers. It has been shown that adding a small amount of long linear chains in a monodisperse linear polymer leads to extension-rate thickening rather than thinning as observed with monodisperse samples [121]. This can be understood by the fact that on one hand, long chains stretch easily, and their contribution to transient hardening is large, while on the other hand, the short chains easily relax and disentangle, which largely reduces the level of the linear envelop as well as the corresponding zero-elongation viscosity [122]; these effects are illustrated in Figure 38a. Further, Figure 38b compares the transient viscosity of two binary blends composed of same long component in the same proportion [122]. Since the short components are too short to be stretched, the steady viscosity of the two samples is identical, while their linear envelop is largely influenced by the molar mass of the short component [122].

5.2.3 Branched Architectures

The elongational behavior of linear and star polymer is similar. In particular, same elongational thinning behavior has also been reported for star polymers [19]. On the other hand, the steady elongational viscosity of complex branched

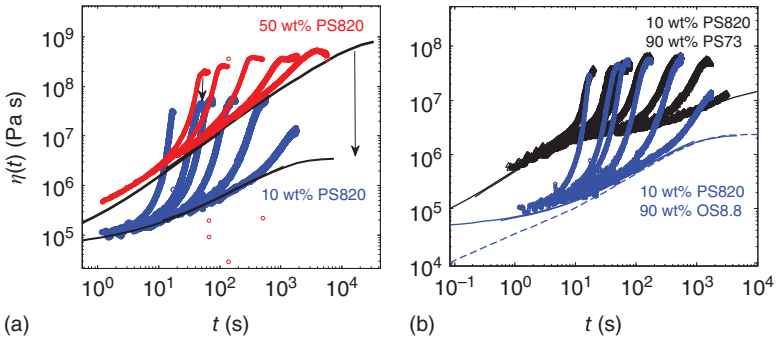

Figure 38 (a) Stress growth coefficient (transient elongational viscosity) and linear viscoelastic envelope (black curve) of a monodisperse linear polystyrene with 820 kg mol^{-1} diluted at 50 wt% (red) or at 10 wt% (blue) in styrene oligomers of 8.8 kg mol^{-1} [45]. Source: Data from T. Shahid, Q. Huang, F. Oosterlinck, C. Clasen, and E. van Ruymbeke, Dynamic dilution exponent in monodisperse entangled polymer solutions, Soft Matter, 13 (1) 269 (2017). (b) Respective data for a monodisperse linear polystyrene with 820 kg mol^{-1} diluted at 10 wt% in styrene oligomers of 8.8 kg mol^{-1} (blue) or in polystyrene of mass 73 kg mol^{-1} (black) [122]. Source: Data from T. Shahid, C. Clasen, F. Oosterlinck, and E. van Ruymbeke, Diluting entangled polymers affects transient hardening but not their steady elongational viscosity, Macromolecules (2019).

polymers with at least two branching points is usually characterized by large extension-rate thickening before eventual thinning [123, 124]. This is explained by the difficulty of chain segments trapped between two branching points to relax their stretch since this can only occur if branching points are moving, i.e. if the branches attached to the branching points are relaxing fast compared to the deformation rate [125]. Figure 39 shows data (a) and an illustration (b) of the influence of the number of generations on strain hardening: the deeper the generation of branch toward the center (see Figure 39), the less the branching points at which they are attached and the higher is a strain hardening [126].

As already mentioned, at very high rates beyond the extension-rate thickening regime, the steady viscosity of complex branched macromolecules reaches the thinning regime characterized by a slope of $-1/2$, similar to that observed for linear polymer melts (Figure 3f) [123, 126, 127]. At this stage, the deformation is so high that the inner generations of the branched molecules reach the maximum stretch which is counterbalanced by the thermal equilibration force of the outer branches attached to the branching point. Therefore, a new relaxation mechanism takes place, according to which the branching points are withdrawn by the stretched backbone, which leads to the stretch saturation [125, 126]. By considering this balance, it was shown that eventually branched polymers with linear backbone (e.g. comb or pom-pom) exhibit identical behavior with linear polymers, provided they have the same equivalent molar mass (or else, the same Rouse time; note that for a branched polymer such as a comb, the Rouse time is an effective one of the dilute backbone once the branches have relaxed) [55, 127].

The influence of the architecture on strain hardening can be further elucidated by taking advantage of the availability or designing well-characterized branched

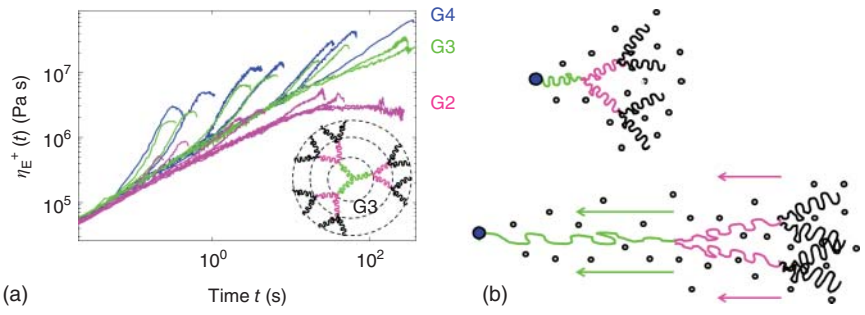

Figure 39 (a) Stress growth coefficient (transient elongational viscosity) of Cayley-tree PMMA polymer melts, composed of 2 (G2), 3 (G3), or 4 (G4) generations. All molecular segments in different generations are identical, each having molar mass of 11 kg mol^{-1} [126]. Source: Data from E. van Ruymbeke, E.B. Muliawan, S.G. Hatzikiriakos, T. Watanabe, A. Hirao, and D. Vlassopoulos, Journal of Rheology 54, 643 (2010). (b) Illustration of the influence of branching generations on the strain-hardening properties. The stretching of the branches largely increases with their depth in their corresponding generation (arrows).

polymers. This is illustrated in Figure 40, where the stress growth coefficients of model comb polymers with varying molecular characteristics are depicted at different Hencky strain rates [128]. Similarly to linear chains, the polystyrene combs exhibit transient strain hardening at stretch rates above the inverse Rouse time. Strain hardening was found to be enhanced and occurred at lower rates when the number of branches or the number of entanglements in the segments between branches is larger. The onset of stretching depends primarily on the number of entanglements per branch and is controlled by the dynamic dilution due to the branches, effectively confirming the abovementioned analogy between combs and linear polymers with the same effective Rouse time accounting for the dilution effect of the hierarchically relaxed branches [55, 127, 128]. These ideas have been incorporated into a pom-pom-based constitutive model which describes quantitatively the extensional response of comb polymers [129].

As in the case of shear flow discussed above, relaxation following cessation of steady elongational flow is an interesting test with rich information and can only be accurately performed with FSR instrumentation [130, 131]. It provides important information on the role of macroscopic structure in the way a deformed polymer releases its stretch; hence, it serves as a useful measure of material performance. A recent comparison of stress relaxation upon cessation or steady shear and elongational flow of the Cayley-tree poly(methyl methacrylate) (PMMA) discussed in the context of Figure 39 above revealed unexpected findings [132]: it was much broader and slower in elongation compared to shear, and it is also slower at higher generations, while it is extension-rate independent for rates below the Rouse rate of the outer segment. These results suggest the presence of strong elastic memory in these materials, and while there is no full theoretical explanation, it appears that the coupling of stretches of different generations is at the origin of the slow and broad relaxation.

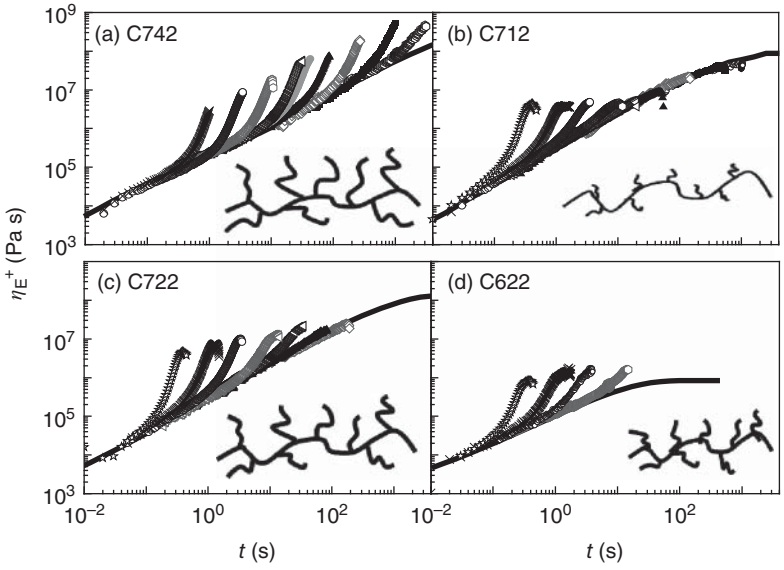

Figure 40 (a,b) Stress growth coefficient of polystyrene comb melts with the same backbone molar mass of 860 kg mol^{-1} (code c7) and the same number of branches [29] but with longer (42 kg mol^{-1}, a) or shorter (12 kg mol^{-1}, b) branches. (c,d) Respective data of polystyrene comb melts with the same number of branches [29] and the same branch molar mass (22 kg mol^{-1}) but with a longer (860 kg mol^{-1}, c) or a shorter (275 kg mol^{-1}, code c6 in d) backbone. Insets attempt at illustrating the differences among samples [128]. Source: H. Lentzakis, D. Vlassopoulos, D. J. Read, H. Lee, T. Chang, P. Driva, N. Hadjichristidis, Uniaxial extensional rheology of well-characterized comb polymers, J. Rheol., 57, 2, 605, https://doi.org/10.1122/1.4789443.

A further critical manifestation of the significance of stress relaxation experiments concerns the much studied difference between the response to elongation of polymer melts and solutions, addressed above. Solutions of short polymers in different solvents were shown to exhibit extension-rate thickening of steady elongational viscosity at intermediate elongational rates if the solvent is molecular or has a small molar mass (e.g. oligomeric), whereas they were only thinning in the case of long polymeric solvent and of course one-component melt [113, 117]. It has been argued that unlike short polymeric solvents, long polymeric solvents promote local nematic interactions, which reduce the resistance to stretching (hence thickening) because of the anisotropic monomeric friction (discussed above) [117]. Relaxation measurements indicated that blends of short polymer in short polymeric solvent relax more slowly at intermediate time than blends of the same polymers in long polymeric solvent, conforming to this scenario [131, 133]. Importantly, ex situ small-angle neutron scattering measurements with appropriately prepared hydrogenated and deuterated polystyrene mixtures confirmed the presence of nematic interactions in the short–long polymer solutions [133].

6 Applications of Industrial Relevance

6.1 Controlling Flow Properties in Industrial Processes

In many industrial processes and applications, polymeric materials undergo complex flows comprising both shear and extensional contributions, hence affecting their properties in a complicated way [1, 2, 8, 134]. Therefore, careful characterization of these materials is necessary to accurately model and predict the processing/application conditions that will lead to optimum final properties of the finished product. Rheology can and has been used as an effective tool to characterize these materials. For example, already in 1979, Meissner reported the film-blowing performance of three different LDPE resins, two of which performed identically, while the third could not be processed at all [135, 136]. All three resins exhibited similar simple shear flow characteristics such as melt flow index (MFI) and (equivalently) zero-shear viscosity. However, the extensional stress growth coefficient was distinctly different, which later was attributed to the differences in the degree of long-chain branching in these materials. Indeed, as discussed in Section 5, subtle changes in molecular architecture (e.g. branching or the presence of a high molar mass tail in the distribution) can influence the extensional properties much more profoundly compared to shear [8]. Extension hardening is usually necessary in industrial processes, since it is known to stabilize the processes, preventing strain localization as well as brittle fracture [134]. On the other hand, strongly shear thinning polymers are favorable for extrusion applications, for example [134]. Therefore, it is important to understand and control how, within the same sample, extension hardening can be enhanced while keeping low shear viscosity. As illustrated in Figure 40, branched polymers such as comb polymers exhibit this combination of extension thickening and shear thinning. Similar behavior is observed with LDPE, which makes them particularly useful in processing applications, as also mentioned in the introduction [8]; therefore, systematic studies of model combs have practical consequences as well [128, 129]. Material and flow characteristics are crucial for analyzing polymer processing. Note, however, that here we do not discuss several important topics such as the properties of semiflexible or rod-like polymers (forming liquid crystalline mesophases) [137], process instabilities (such as wall slip [10, 138, 139] and shear banding [8, 36, 140]), or fracture mechanisms [1, 141, 142] and flow-induced crystallization [143, 144].

6.2 Rheology as a Characterization Tool

As explained in Section 4, the viscoelastic properties of a polymer melt strongly depend on its composition. Therefore, given its high sensitivity, rheology is often used as a reliable quantitative tool to determine the architectures present in complex polymeric materials. This remains a current trend in the field; nevertheless, we illustrate its importance with some selected examples below.

6.2.1 Detection of Long-Chain Branching

Rheology has been used to detect low levels of long-chain branching [145–147]. By comparing the experimental viscoelastic data of lightly branched polymers

with the rheology predicted by assuming that all chains are linear, it is possible to estimate the level of branching chains in the sample. Furthermore, several studies with polyethylene samples have inferred the presence of complex molecules from the thermorheological complexity of the material [145, 148]. In general, models such as the tube models, which determine the rheological properties from the sample composition, are very useful since they allow validating the composition of a sample, determined by means of SEC/LS analysis or NMR. Besides linear rheology, several recent investigations have shown the huge sensitivity of elongational rheology to macromolecular architecture, hence its potential to highlight the presence of such complex polymers [8, 123]. In particular, the strain hardening observed in extension can give us important information about the branching level and seniority of the macromolecules. Quantitative models able to predict the nonlinear behavior of polymer melts will certainly be further developed in the near future.

6.2.2 Inverse Problem: From Rheology to Polymer Composition

While the MMD of a complex branched polymer can be determined experimentally (say by means of SEC), its interpretation in terms of different architectures contributing to the experimental signal is far from trivial. The reason is that different architectures could produce virtually the same signal. Hence, associating MMD to molecular structure remains a formidable challenge. In order to reduce the ill-posed character of this exercise, it is necessary to exploit any information available from the synthesis protocol [67, 68]. Similarly, determining the composition of a polymer only from its viscoelastic curves is an ill-posed problem: several compositions can lead to same linear viscoelastic behavior; hence, there is no unique solution. However, by combining information from the synthesis scheme with rheological results, it is possible to reduce the number of possible realistic solutions and even to solve the problem unambiguously if the entire sample composition can be described based only on few parameters, thus minimizing the number of possible solutions (i.e. uncertainty). For example, it has been shown that the MMD of a linear polymer can be determined from its viscoelastic properties as long as we know a priori that a sample is linear [149, 150], and that the unknown MMD can be described by one or two log-normal distributions or generalized exponential (GEX) functions. In this way, the number of unknown parameters is low enough (two parameters by log-normal and three by GEX function) to overcome the ill-posed properties of the inverse problem. The parameters related to the MMD can then be determined by means of a least-square minimization, by comparing the experimental moduli to the one predicted from the hypothetical MMD. Such inverse modeling is particularly useful for linear polymers that cannot be measured by SEC due to their insolubility in adequate solvent or due to their very high molar mass, outside the experimental validity window. With randomly branched architectures, the inverse modeling is only possible when the specific synthetic methodology used is known and by combining information with SEC/LS and viscoelastic data. Furthermore, a statistical approach is often needed to interpret the data. For example, as discussed in Section 4.3, the composition of randomly branched polymers that follow Monte Carlo statistics and for which the monomeric composition is known can be well

described by very few parameters (mainly the conversion level) [68]. In this case, the unknown parameters can be determined by inverse modeling of the linear viscoelasticity (LVE) data. Another example is branched polymers obtained by coupling linear chains by means of coupling agents [67]. If the MMD of the linear parents is known, one can determine the MMD corresponding to each possible architecture present in the final sample. Thus, the only unknown parameters are the relative fraction of these architectures, which can be determined from the linear rheology (or from the MMD) of the branched polymer. However, in general, the problem remains challenging, and recent progress is due to the availability of advanced characterization techniques such as interaction chromatography that support rheology and the classic SEC [66, 151].

7 Summary

The purpose of this chapter has been to provide the necessary ingredients for appreciating and eventually understanding the viscoelastic properties of branched polymers that set them apart from other materials and make them particularly useful in applications. The basic elements of linear and nonlinear rheology have been presented, along with a detailed description of the mechanics that govern the linear viscoelastic response of linear and star polymers. Then, it has been shown by means of selected examples that branched polymer viscoelasticity can be understood on the basis of linear and star response, with two additional elements, the hierarchical relaxation and the associated dynamic dilution. The nonlinear rheology is more complex, with more outstanding challenges. However, the same framework applies for understanding and analyzing branched polymers: based on the knowledge of linear (in particular) polymers and stars, with the additional ideas of dilution and branch point withdrawal. The state-of-the-art modeling and experimental approaches have been presented. Simulations have not been addressed in detail, but appropriate references are cited where needed. Mixtures have been discussed in the context of CR. A number of other intriguing phenomena such as flow instabilities and flow-induced crystallization are not covered. An important aspect of the discussion is the link of macroscopic rheological features to molecular characteristics, which is the concept behind "macromolecular" rheology. The latter can serve as a tool for material design or process optimization. It is hoped that this review will serve as a useful reference and motivate further discussions and investigations in this fascinating field.

References

1 Denn, M.M. (2008). *Polymer Melt Processing*. Cambridge: Cambridge University Press.
2 Wilkinson, A.N. and Ryan, A.J. (1999). *Polymer Processing and Structure Development*. Kluwer Academic Publishers.

3 Doi, M. and Edwards, S.F. (1986). *The Theory of Polymer Dynamics*. Oxford: Oxford University Press.
4 Dealy, J.M., Read, D.J., and Larson, R.G. (2018). *Structure and Rheology of Molten Polymers*, 2e. Hanser. doi: 10.3139/9781569906125.
5 Pipkin, A.C. (1986). *Lectures on Viscoelasticity Theory*. Springer.
6 Ferry, J.D. (1980). *Viscoelastic Properties of Polymers*, 3e. Wiley.
7 Rubinstein, M. and Colby, R.H. (2003). *Polymer Physics*. Oxford: Oxford University Press.
8 Wang, S.-Q. (2017). *Nonlinear Polymer Rheology: Macroscopic Phenomenology and Molecular Foundation*. Wiley.
9 Graessley, W.W. (2008). *Polymeric Liquids and Networks: Dynamics and Rheology*. Garland.
10 Hatzikiriakos, S.G. (2012). *Progr. Polym. Sci.* 37: 624–643. doi: 10.1016/j.progpolymsci.2011.09.004.
11 Schweizer, T. and Schmidheiny, W. (2013). *J. Rheol.* 57 (3): 841–856. doi: 10.1122/1.4797458.
12 Costanzo, S., Huang, Q., Ianniruberto, G. et al. (2016). *Macromolecules* 49: 3925–3935. doi: 10.1021/ma301368d.
13 Hemingway, E.J., Kusumaatmaja, H., and Fielding, S.M. (2017). *Phys. Rev. Lett.* 119: 028006. doi: 10.1103/PhysRevLett.119.028006.
14 Snjikers, F. and Vlassopoulos, D. (2011). *J. Rheol.* 55 (6): 1167–1186. doi: 10.1122/1.3625559.
15 Schweizer, T. and Stöckli, M. (2008). *J. Rheol.* 52: 713–727. doi: 10.1122/1.2896110.
16 Costanzo, S., Ianniruberto, G., Marrucci, G., and Vlassopoulos, D. (2018). *Rheol. Acta* 57: 363–376. doi: 10.1007/s00397-018-1080-1.
17 Bach, A., Rasmussen, H.K., and Hassager, O. (2003). *J. Rheol.* 47: 429–441. doi: 10.1122/1.1545072.
18 Sentmanat, M.L. (2004). *Rheol. Acta* 43: 657–669. doi: 10.1007/s00397-004-0405-4.
19 Huang, Q., Agostini, S., Hengeller, L. et al. (2016). *Macromolecules* 49: 6694–6699. doi: 10.1021/acs.macromol.6b01348.
20 van Ruymbeke, E., Keunings, R., and Bailly, C. (2005). *J. Nonnewton Fluid Mech.* 128 (1): 7–22. doi: 10.1016/j.jnnfm.2005.01.006.
21 van Ruymbeke, E., Vlassopoulos, D., Kapnistos, M. et al. (2010). *Macromolecules* 43: 525–531. doi: 10.1021/ma901229f.
22 Park, S.J., Desai, P.S., Chen, X., and Larson, R.G. (2015). *Macromolecules* 48: 4122–4131. doi: 10.1021/ma5024632.
23 Cloitre, M. and Vlassopoulos, D. (2012). In: *Applied Polymer Rheology. Polymeric Fluids with Industrial Applications* (ed. M. Kontopoulou), 209–242. John Wiley & Sons, Inc.
24 Han, C.D., Baek, D.H., Kim, J.K. et al. (1995). *Macromolecules* 28: 5043–5062. doi: 10.1021/ma00118a038.
25 Xie, R., Lee, Y., Aplan, M.P. et al. (2017). *Macromolecules* 50: 5146–5154. doi: 10.1021/acs.macromol.7b00712.
26 Colby, R.H. (1989). *Polymer* 30 (7): 1275–1278. doi: 10.1016/0032-3861(89)90048-7.

27 Kapnistos, M., Hinrichs, A., Vlassopoulos, D. et al. (1996). *Macromolecules* 29: 7155–7163. doi: 10.1021/ma960835n.
28 Kapnistos, M., Vlassopoulos, D., Roovers, J., and Leal, L.G. (2005). *Macromolecules* 38: 7852–7862. doi: 10.1021/ma050644x.
29 McLeish, T.C.B. (2002). *Adv. Phys.* 51 (6): 1379–1529. doi: 10.1080/00018730210153216.
30 van Gurp, M. and Palmen, J. (1998). *Rheol. Bull.* 65: 5–8.
31 Abdel-Goad, M., Pyckhout-Hintzen, W., Kahle, S. et al. (2004). *Macromolecules* 37: 8135–8144. doi: 10.1021/ma030557.
32 Liu, C.Y., He, J., Keunings, R., and Bailly, C. (2006). *Macromolecules* 39: 8867. doi: 10.1021/ma061969w.
33 Liu, C., He, J., van Ruymbeke, E. et al. (2006). *Polymer* 47: 4461–4477. doi: 10.1016/j.polymer.2006.04.054.
34 Szántó, L., Vogt, R., Meier, J. et al. (2017). *J. Rheol.* 61: 1023–1033. doi: 10.1122/1.4998174.
35 Coppola, S., Grizzuti, N., Floudas, G., and Vlassopoulos, D. (2007). *J. Rheol.* 51 (5): 1007–1025. doi: 10.1122/1.2751076.
36 Snijkers, F., Pasquino, R., Olmsted, P.D., and Vlassopoulos, D. (2015). *J. Phys.: Condens. Matt.* 27: 473002. doi: 10.1088/0953-8984/27/47/473002.
37 Likhtman, A.E. and McLeish, T.C.B. (2002). *Macromolecules* 35: 6332–6343. doi: 10.1021/ma0200219.
38 Larson, R.G., Sridhar, T., Leal, L.G. et al. (2003). *J. Rheol.* 47: 809. doi: 10.1122/1.1567750.
39 Fetters, L.J., Lohse, D.J., and Colby, R.H. (2007). *Physical Properties of Polymers Handbook* (ed. J.E. Mark), 447–454. Springer.
40 Shchetnikava, V., Slot, J., and van Ruymbeke, E. (2019). *Polymers* 11 (5): 754. doi: 10.3390/polym11050754.
41 Watanabe, H. (2008). *Progr. Theor. Phys. Suppl.* 175: 17–26.
42 des Cloizeaux, J. (1988). *Europhysics Letters* 5: 5.
43 Marrucci, G. and Polym, J. (1985). *Sci.: Polym. Phys. Ed.* 23: 159–177. doi: 10.1002/pol.1985.180230115.
44 Colby, R.H. and Rubinstein, M. (1990). *Macromolecules* 23: 2753–2757. doi: 10.1021/ma00212a028.
45 Shahid, T., Huang, Q., Oosterlinck, F. et al. (2017). *Soft Matter* 13 (1): 269. doi: 10.1039/C6SM01083K.
46 van Ruymbeke, E., Shchetnikava, V., Matsumiya, Y., and Watanabe, H. (2014). *Macromolecules* 47 (21): 7653–7665. doi: 10.1021/ma501566w.
47 Watanabe, H., Ishida, S., Matsumiya, Y., and Inoue, T. (2004). *Macromolecules* 37 (5): 1937–1951. doi: 10.1021/ma030443y.
48 Read, D.J., Shivokhin, M.E., and Likhtman, A.E. (2018). *J. Rheol.* 62: 1017. doi: 10.1122/1.5031072.
49 Viovy, J.L., Rubinstein, M., and Colby, R. (1991). *Macromolecules* 24 (12): 3587–3596. doi: 10.1021/ma00012a020.
50 Watanabe, H., Matsumiya, Y., and van Ruymbeke, E. (2013). *Macromolecules* 46 (23): 9296–9312. doi: 10.1021/ma4018795.
51 Struglinski, M.J. and Graessley, W.W. (1985). *Macromolecules* 18: 2630–2643. doi: 10.1021/ma00154a046.

52 Liu, C.-Y., Keunings, R., and Bailly, C. (2006). *Phys. Rev. Lett.* 97: 246001. doi: 10.1103/PhysRevLett.97.246001.

53 Park, S.J. and Larson, R.G. (2004). *Macromolecules* 37 (2): 597–604. doi: 10.1021/ma0343683.

54 van Ruymbeke, E., Liu, C.-Y., and Bailly, C. (2007). *Rheology Reviews*, 53–134. The British Society of Rheology.

55 Lentzakis, H., Costanzo, S., Vlassopoulos, D. et al. (2019). *Macromolecules* 52: 3010–3028. doi: 10.1021/acs.macromol.9b00251.

56 Ball, R.C. and McLeish, T.C.B. (1989). *Macromolecules* 22 (4): 1911–1913. doi: 10.1021/ma00194a066.

57 Frischknecht, A.L., Milner, S.T., Pryke, A. et al. (2002). *Macromolecules* 35: 4801–4820. doi: 10.1021/ma0101411.

58 Lee, J.H., Fetters, L.J., and Archer, L. (2005). *Macromolecules* 38: 4484–4494. doi: 10.1021/ma047687i.

59 Roovers, J. (1985). *Polymer* 26: 1091–1095. doi: 10.1016/0032-3861(85)90234-4.

60 Fetters, L.J., Kiss, A.D., Pearson, D.S. et al. (1993). *Macromolecules* 27: 647–654. doi: 10.1021/ma00056a015.

61 Vlassopoulos, D., Fytas, G., Pakula, T., and Roovers, J. (2001). *J. Phys.: Condens. Matt.* 13: R855–R876. PII: S0953-8984(01)19758-4.

62 van Ruymbeke, E., Bailly, C., Keunings, R., and Vlassopoulos, D. (2006). *Macromolecules* 39 (18): 6248–6259. doi: 10.1021/ma0604385.

63 van Ruymbeke, E., Orfanou, K., Kapnistos, M. et al. (2007). *Macromolecules* 40: 5941–5952. doi: 10.1021/ma0706024.

64 Larson, R.G. (2001). *Macromolecules* 34 (13): 4556–4571. doi: 10.1021/ma000700o.

65 Ahmadi, M., Pioge, S., Fustin, C.A. et al. (2017). *Soft Matter* 13: 1063–1073. doi: 10.1039/C6SM02576E.

66 van Ruymbeke, E., Lee, H., Chang, T. et al. (2014). *Soft Matter* 10: 4762–4777. doi: 10.1039/c4sm00105b.

67 van Ruymbeke, E., Coppola, S., Balacca, L. et al. (2010). *J. Rheol.* 54: 507–538. doi: 10.1122/1.3368729.

68 Van Ruymbeke, E., Slot, J.J.M., Kapnistos, M., and Steeman, P.A.M. (2013). *Soft Matter* 9 (29): 6921–6935. doi: 10.1039/C3SM50226K.

69 Tobita, H. (2001). *J. Polym. Sci. B Polym. Phys.* 39 (4): 391–403. doi: 10.1002/1099-0488(20010115)39:4<391::AID-POLB1011>3.0.CO;2-3.

70 Das, C., Inkson, N.J., Read, D.J., and Kelmanson, M.A. (2006). *J. Rheol.* 50: 207. doi: 10.1122/1.2167487.

71 Read, D.J., Auhl, D., Das, C. et al. (2011). *Science* 333 (6051): 1871–1874. doi: 10.1126/science.1207060.

72 Chen, X., Rahman, M.S., Lee, H. et al. (2011). *Macromolecules* 44 (19): 7799–7809. doi: 10.1021/ma2011377.

73 Wang, Z., Chen, X., and Larson, R. (2010). *J. Rheol.* 54: 223. doi: 10.1122/1.3301246.

74 Inkson, N.J., Graham, R.S., McLeish, T.C.B. et al. (2006). *Macromolecules* 39 (12): 4217–4227. doi: 10.1021/ma060018f.

75 Ahmadi, M., Bailly, C., Keunings, R. et al. (2011). *Macromolecules* 44 (3): 647–659. doi: 10.1021/ma102041h.

76 Blackwell, R.J., Harlen, O.G., and McLeish, T.C.B. (2001). *Macromolecules* 34 (8): 2579–2596. doi: 10.1021/ma001687a.

77 Cox, W.P. and Merz, E.H. (1958). *J. Polym. Sci.* 28 (118): 619–622. doi: 10.1002/pol.1958.1202811812.

78 Winter, H.H. (2009). *Rheol. Acta* 48: 241–243. doi: 10.1007/s00397-008-0329-5.

79 Snijkers, F. and Vlassopoulos, D. (2014). *Rheol. Acta* 53: 935–946. doi: 10.1007/s00397-014-0799-6.

80 Snijkers, F., Ratkanthwar, K., Vlassopoulos, D., and Hadjichristidis, N. (2013). *Macromolecules* 46: 5702–5713. doi: 10.1021/ma400662b.

81 Rabin, Y. and Öttinger, H.C. (1990). *Europhys. Lett.* 13: 423. doi: 10.1209/0295-5075/13/5/008.

82 Colby, R.H., Boris, D., Krause, W.E., and Dou, S. (2007). *Rheol. Acta* 46: 569. doi: 10.1007/s00397-006-0142-y.

83 Graessley, W.W. (1974). *Adv. Polym. Sci.* 16: 1–179. doi: 10.1007/BFb0031037.

84 Stratton, R.A. (1972). *Macromolecules* 5: 304. doi: 10.1021/ma60027a015.

85 Jeong, S.H., Kim, J.M., and Baig, C. (2017). *Macromolecules* 50 (11): 4491–4500. doi: 10.1021/acs.macromol.7b00544.

86 Xu, X., Chen, J., and An, L. (2014). *J. Chem. Phys.* 140: 174902. doi: 10.1063/1.4873709.

87 Baig, C., Mavrantzas, V., and Kröger, M. (2010). *Macromolecules* 43 (16): 6886–6902. doi: 10.1021/ma100826u.

88 Subbotin, A., Semenov, A., Manias, E. et al. (1995). *Macromolecules* 28: 3898–3900. doi: 10.1021/ma00115a021.

89 Bird, R.B., Curtiss, C.F., Armstrong, R.C., and Hassager, O. (1987). *Dynamics of Polymeric Liquids, Vol. 2: Kinetic Theory*. Wiley, New York.

90 Larson, R.G. (2005). *J. Rheol.* 49: 1. doi: 10.1122/1.1835336.

91 Marrucci, G. (1996). *J. Non-Newtonian Fluid Mech.* 62: 279. doi: 10.1016/0377-0257(95)01407-1.

92 Ianniruberto, G. and Marrucci, G. (2002). *J. Non-Newtonian Fluid Mech.* 102: 383–395. doi: 10.1016/S0377-0257(01)00188-4.

93 Ianniruberto, G. (2015). *J. Rheol.* 59: 211. doi: 10.1122/1.4903495.

94 Graham, R.S., Likhtman, A.E., McLeish, T.C.B., and Milner, S.T. (2003). *J. Rheol.* 47: 1171. doi: 10.1122/1.1595099.

95 Nafar Sefiddashti, M.H., Edwards, B.J., and Khomami, B. (2015). *J. Rheol.* 59: 119. doi: 10.1122/1.4903498.

96 Yaoita, T., Isaki, T., Masubuchi, Y. et al. (2012). *Macromolecules* 45: 2773–2782. doi: 10.1021/ma202525v.

97 Schweizer, T., van Meerveld, J., and Ottinger, H.C. (2004). *J. Rheol.* 48: 1345. doi: 10.1122/1.1803577.

98 Hieber, C.A. and Chiang, H.H. (1989). *Rheol. Acta* 28: 321. doi: 10.1007/BF01329342.

99 Nafar Sefiddashti, M.H., Edwards, B.J., and Khomami, B. (2019). *Macromolecules* 52: 8124–8143. doi: 10.1021/acs.macromol.9b01099.

100 Schweizer, K.S., Xie, S.-J. (2018). *ACS Macro Lett.* 7: 218–222. doi: 10.1021/acsmacrolett.7b00882.

101 Parisi, D., Costanzo, S., Jeong, Y., Ahn, J. et al. (2021). *Macromolecules* 54: 2811–2827. doi: 10.1021/acs.macromol.0c02839.

102 Tanner, R.I. and Keentok, M. (1983). *J. Rheol.* 27: 47–57. doi: 10.1122/1.549698.

103 Snijkers, F., Vlassopoulos, D., Ianniruberto, G. et al. (2013). *ACS Macro Lett.* 2: 601–604. doi: 10.1021/mz400236z.

104 Auhl, D., Ramirez, J., Likhtman, A.E. et al. (2008). *J. Rheol.* 52 (3): 801–835. doi: 10.1122/1.2890780.

105 Watanabe, H., Matsumiya, Y., Sato, T. (2021). *Macromolecules* 54: 3700–3715. doi: 10.1021/acs.macromol.1c00013.

106 Ianniruberto, G. and Marrucci, G. (2020). *Macromolecules* 53: 1338–1345. doi: 10.1021/acs.macromol.9b02330.

107 Fitzgerald, B.W., Lentzakis, H., Sakellariou, G. et al. (2014). *J. Chem. Phys.* 141: 114907. doi: 10.1063/1.4895610.

108 Santagelo, P.G. and Roland, C.M. (2001). *J. Rheol.* 45: 583–594. doi: 10.1122/1.1349711.

109 Snijkers, F., Vlassopoulos, D., Lee, H. et al. (2013). *J. Rheol.* 57: 1079. doi: 10.1122/1.480419893.

110 Bach, A., Almdal, K., Rasmussen, H.K., and Hassager, O. (2003). *Macromolecules* 36: 5174–5179. doi: 10.1021/ma034279q.

111 Matsumiya, Y., Watanabe, H., Masubuchi, Y. et al. (2018). *Macromolecules* 51: 9710–9729. doi: 10.1021/acs.macromol.8b01954.

112 Sridhar, T., Acharya, M., Nguyen, D.A., and Bhattacharjee, P.K. (2014). *Macromolecules* 47: 379–386. doi: 10.1021/ma401213r.

113 Huang, Q., Hengeller, L., Alvarez, N.J., and Hassager, O. (2015). *Macromolecules* 48: 4158–4163. doi: 10.1021/acs.macromol.5b00849.

114 Bhattacharjee, P.K., Oberhauser, J.P., McKinley, G.H., and Sridhar, T. (2002). *Macromolecules* 35: 10131–10148. doi: 10.1021/ma0118623.

115 Huang, Q., Mednova, O., Rasmussen, H.K. et al. (2013). *Macromolecules* 46: 5026. doi: 10.1021/ma4008434.

116 Lindeblad Wingstrand, S., Alvarez, N.J., Huang, Q., and Hassager, O. (2015). *Phys. Rev. Lett.* 115: 078302.

117 Huang, Q., Alvarez, N.J., Matsumiya, Y. et al. (2013). *ACS Macro Lett.* 2: 741–744. doi: 10.1021/mz400319v.

118 Marrucci, G. and Ianniruberto, G. (2004). *Macromolecules* 37: 3934–3942. doi: 10.1021/ma035501u.

119 O'Connor, T.C., Alvarez, N.J., and Robbins, M.O. (2018). *Phys. Rev. Lett.* 121: 04701. doi: 10.1103/PhysRevLett.121.047801.

120 Masubuchi, Y., Takimoto, J.I., Koyama, K. et al. (2001). *J. Chem. Phys.* 115: 4387. doi: 10.1063/1.1389858.

121 Nielsen, J.K., Rasmussen, H.K., Hassager, O., and McKinley, G.H. (2006). *J. Rheol.* 50: 453–476. doi: 10.1122/1.2206711.

122 Shahid, T., Clasen, C., Oosterlinck, F., and van Ruymbeke, E. (2019). *Macromolecules* doi: 10.1021/acs.macromol.8b02701.

123 Nielsen, J.K., Rasmussen, H.K., Denberg, M. et al. (2006). *Macromolecules* 39: 8844–8853. doi: 10.1021/ma061476r.

124 Laun, H.M. and Schuch, H. (1989). *J. Rheol.* 33 (1): 119. doi: 10.1122/1.550058.

125 McLeish, T.C.B. and Larson, R.G. (1998). *J. Rheol.* 42: 81–110. doi: 10.1122/1.550933.

126 van Ruymbeke, E., Muliawan, E.B., Hatzikiriakos, S.G. et al. (2010). *J. Rheol.* 54: 643. doi: 10.1122/1.3368724.

127 Ianniruberto, G. and Marrucci, G. (2013). *Macromolecules* 46: 267–275. doi: 10.1021/ma302131b.

128 Lentzakis, H., Vlassopoulos, D., Read, D.J. et al. (2013). *J. Rheol.* 57 (2): 605. doi: 10.1122/1.4789443.

129 Lentzakis, H., Das, C., Vlassopoulos, D., and Read, D.J. (2014). *J. Rheol.* 58: 1855–1875. doi: 10.1122/1.4895606.

130 Nielsen, J.K., Rasmussen, H.K., and Hassager, O. (2008). *J. Rheol.* 52: 885–899. doi: 10.1122/1.2930872.

131 Hengeller, L., Huang, Q., Dorokhin, A. et al. (2016). *Rheol. Acta* 55: 303–314. doi: 10.1007/s00397-016-0916-9.

132 Huang, Q., Costanzo, S., Das, C., and Vlassopoulos, D. (2017). *J. Rheol.* 61: 35–47. doi: 10.1122/1.4966040.

133 Kirkensgaard, J.J.K., Hengeller, L., Dorokhin, A. et al. (2016). *Phys. Rev. E* 94: 020502(R). doi: 10.1103/PhysRevE.94.020502.

134 Baird, D. and Collias, D. (2014). *Polymer Processing: Principles and Design*. Wiley.

135 Wagner, M.H., Raible, T., and Meissner, J. (1979). *Rheol. Acta* 427–428. doi: 10.1007/BF01515835.

136 Raible, T., Demarmels, A., and Meissner, J. (1979). *Polym. Bull.* 1: 397–402. doi: 10.1007/BF00284409.

137 Mewis, J. and Moldenaers, P. (1996). *Curr. Opinion Colloid Interface Sci.* 1 (4): 466–471. doi: 10.1016/S1359-0294(96)80114-2.

138 Hatzikiriakos, S.G. (2015). *Soft Matter* 11: 7851–7856. doi: 10.1039/c5sm01711d.

139 Awati, K.M., Park, Y., Weisser, E., and Mackay, M.E. (2000). *J. Non-Newtonian Fluid Mech.* 89: 117–131.

140 Olmsted, P. (2008). *Rheol. Acta* 47: 283. doi: 10.1007/s00397-008-0260-9.

141 Creton, C. and Ciccotti, M. (2016). *Rep. Progr. Phys.* 79: 046601. doi: 10.1088/0034-4885/79/4/046601.

142 Huang, Q. and Hassager, O. (2017). *Phys. Rev. Lett.* 13: 3470–3474. doi: 10.1039/c7sm00126f.

143 Hamad, F.G., Colby, R.H., and Milner, S.T. (2015). *Macromolecules* 48: 3725–3738. doi: 10.1021/acs.macromol.5b00386.

144 Graham, R.S. (2019). *J. Rheol.* 63: 203. doi: 10.1122/1.5056170.

145 Wood-Adams, P.M. and Dealy, J.M. (2000). *Macromolecules* 33: 7481–7488. doi: 10.1021/ma991534r.

146 Derakhshandeh, M., Ansari, M., Doufas, A.K., and Hatzikiriakos, S.G. (2017). *Polym. Test.* 60: 68–77. doi.org/10.1016/j.polymertesting.2017.03.010.

147 Hatzikiriakos, S.G. (2000). *Polym. Eng. Sci.* 40: 2279–2287.

148 van Ruymbeke, E., Stephenne, V., Daoust, D. et al. (2005). *J. Rheol.* 49: 1503. doi: 10.1122/1.2048743.

149 Leonardi, F., Allal, A., and Marin, G. (1998). *Rheol. Acta* 3: 199–213. doi: 10.1007/s003970050108.

150 Carrot, C. and Guillet, J. (1997). *J. Rheol.* 41: 1203–1220. doi: 10.1122/1.550815.

151 Chang, T. (2005). *J. Polym. Sci: Part B: Polym. Phys.* 43: 1591–1607. doi: 10.1002/polb.20440.